



**Semi Arid Land Surface-Atmosphere project.
(SALSA)**

**An overview of changing surface processes in semiarid
grasslands of the San Pedro catchment near Cananea-
Sonora, Mexico.**

**Analisis de los Procesos de Evolucion de las Superficies
(suelo-vegetacion) en region semiarida,
Rio San Pedro - Sonora, Mexico.**

REPORT of the CAMPAIGN 1996-1997

INFORME de ACTIVIDAD 1996-1997.

Monteny B.A.* Lopez Morales J.P.* Elguero E.¹ and Lhomme J.P.*

* ORSTOM-DICTUS : Universidad de Sonora, A.P.1819, Hermosillo-SONORA

¹ ORSTOM-IMADES : Instituto del Medio Ambiente y del Desarrollo

Sustentable en el Estado de Sonora, Hermosillo - SON.

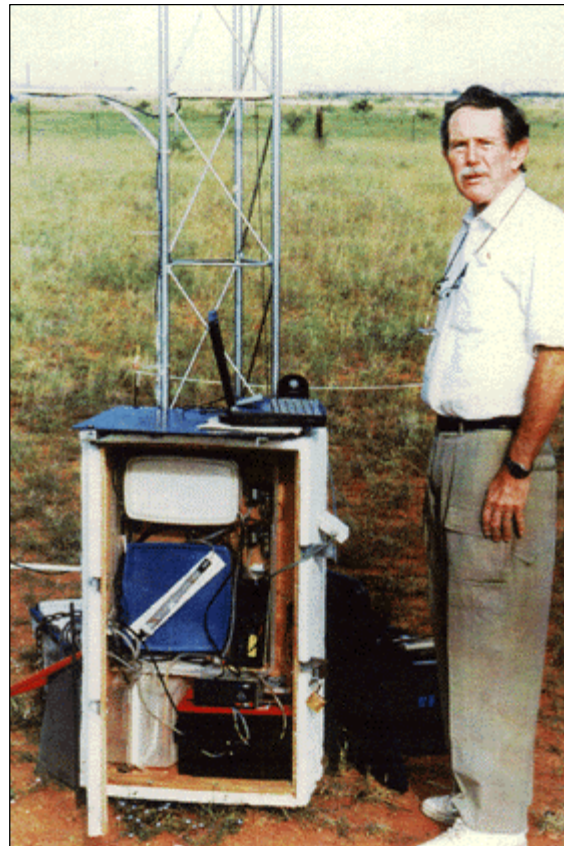
December 1997

A. Contenido

- 1. OBJETIVO**
- 2. METAS**
- 3. RESUMEN**

B. Contents

- 1. INTRODUCTION**
- 2. CHARACTERISTICS OF THE CATCHMENT AREA**
 - 2.1. Catchment area and Sites description**
 - 2.2. Northeastern Sonora climate**
 - 2.3. Vegetation and soil**
- 3. EXPERIMENTAL METHODS**
 - 3.1. Regional climate - Weather station near Morelos**
 - 3.2. Radiation budget**
 - 3.3. Available energy ($R_n - G$)**
 - 3.4. Precipitation / soil moisture availability**
 - 3.5. Small scale variability**
 - 3.6. Soil-vegetation-atmosphere interaction**
- 4. PRELIMINARY RESULTS AND INTERPRETATION**
 - 4.1. Morelos site climatic characteristics**
 - 4.2. Precipitation / soil moisture availability**
 - 4.3. Vegetation : areal biomass production**
 - 4.4. Radiation budget over sparse vegetation**
 - 4.5. Available energy ($R_n - G$)**
 - 4.6. Soil-vegetation-atmosphere interaction: fluxes measurements**
 - 4.7. Scale variability**



Dr. Bruno Monteny, principal investigator, collecting data from the grassland flux station near Ejido Morelos.

OBJETIVO : Evaluación y caracterización de los procesos de evolución de los estados de superficie en zona semiárida para una mejor adecuación entre el recurso y el manejo.

2. Metas:

1. Determinar los principales mecanismos que provocan un cambio en los estados de superficie (degradación-regeneración) de acuerdo con la conjunción de los factores;
2. Entender el nivel de perturbación del funcionamiento de las coberturas vegetales y las consecuencias de su dinamismo (hierba>>suelo desnudo; hierba>>arbusto);
3. Determinar el impacto de las modificaciones de los estados de superficie en el balance radiativo (efecto “feedback”) y por consiguiente en el clima regional.

3. Resumen

Una cobertura vegetal es un sistema dinámico que evoluciona en el tiempo y en el espacio. Nuestras investigaciones se centrarán en las interacciones entre los procesos físicos y el comportamiento biológico de las coberturas vegetales a diferentes escalas espacio-temporales.

Con el fin de percibir la evolución de los estados de superficie (representada por el conjunto cubierta vegetal + suelo), la selección se llevará a cabo, a escala espacial, entre las características del suelo (nivel local) y las de la cuenca y, a escala temporal, entre la estación y la década. El funcionamiento espacial de los estados de superficie en las diferentes escalas temporales será igualmente considerado.

Para lograr este objetivo es necesario caracterizar las variables más importantes, en función de las diferentes escalas espaciotemporales, que deben considerarse para describir la evolución de los estados de superficie observada. De esta manera será posible analizar los mecanismos biogeofísicos que provocan ya sea la degradación, o la regeneración de los estados de superficie. Variables que deben considerarse :

* a nivel del balance radiativo : $R_n = R_s - aR_s + \epsilon R_a - \epsilon\sigma T_s^4$

=> la evolución espacio-temporal de los términos del balance radiativo, modificados por las condiciones de superficie (aR_s y $\epsilon\sigma T_s^4$), permitirá evaluar el impacto de los cambios de estados de superficie en ciertas características de las masas de aire (temperatura nocturna, temperatura del suelo, energía disponible...);

=> la fracción de energía disponible **Rn-G**, debida a los estados de superficie, debe medirse correctamente con el fin de estimar con precisión los intercambios de evaporación **LEv** de los sistemas dispersos;

<p>CLIMA Precipitación (cantidad y distribución) Radiación Temperatura</p>	<p>CICLO AGUA $P = R + Ev + I \pm \partial S$ ¿repartición de lluvias? CICLO CARBONO fotosíntesis : Ph respiración</p>	<p>SUELO estructura, porosidad humedad ¿infiltración de agua de lluvias? PRODUCCION (Ph) materia orgánica</p>
<p>Perturbación externa ¿climática? ¿antrópica? aRs o $\epsilon\sigma Ts^4$</p>	<p>BALANCE de Radiación : Rn $Rs - aRs + \epsilon Ra - \epsilon\sigma Ts^4$ BALANCE de ENERGIA $Rn - G$ = $LEv + H + (Ph)$</p>	<p>¿temperatura? ¿competición para materia orgánica? vacas <> comejens</p>
<p>Estado de equilibrio // sistema unitario del paisaje en el cuenca</p>	<p>Cambio en la distribución del agua > mas chorreo : R menos infiltración : I induce otra distribución de la energía disponible => $Rn - G$</p>	<p>Modificación : ->> de la cobertura vegetal (composición, crecimiento...) ->> del suelo (caracteristicos fisicos y estructura) induce otra repartición de la energía => $Lev + H$</p>
<p>Nivelación que genera otra sistema unitario en el paisaje</p>		

* a nivel del ciclo del agua

$$P = R + I + Ev \pm \partial S$$

y del balance de energía :

$$LEv = Rn - G - H$$

=> la distribución espacio-temporal de las lluvias a escala del ecosistema (escala local) deberá conocerse detalladamente ya que los diferentes flujos de agua en el sistema unitario (distribución del escurrimiento en superficie **R**, reservas hídricas **S**, evaporación **LE_v** dependen de ella;

=> analizar conjuntamente la respuesta del ecosistema (evolución del sistema de raíces profundas, crecimiento de las especies dominantes del ecosistema...) y los intercambios **LE_v** en función de las reservas hídricas del suelo **S** para caracterizar los mecanismos que generan cambios en las interacciones.

* a nivel del ecosistema:

analizar la evolución espaciotemporal de la composición florística y llevar a cabo el seguimiento de la actividad biológica de los sistemas unitarios (producción de materia orgánica subterránea y aérea, índice foliar, grado de recubrimiento de la superficie del suelo y altura...), así como de las reservas de materia orgánica presentes en el suelo;

* a escala del transecto,

la transferencia lateral del agua de lluvia en el paisaje (paso de un sistema unitario a otro) constituye un parámetro importante que deberá evaluarse debido a la heterogeneidad espaciotemporal del medio (variaciones a gran escala de las reservas hídricas del suelo).

¿Qué criterios se utilizan para distinguir los sistemas unitarios del paisaje?
--

Considerando el aspecto general de la cuenca y tomando un transecto que va del piedemonte hasta la hondonada (escurrimiento), pueden observarse 4 grandes sistemas unitarios:

zona de piedemonte: suelo estructurado, bastante profundo, rico en humus con una cobertura vegetal de dos estratos: herbáceo (plantas perennes y anuales) y arbustivas (mesquites con palmitas + yucas);

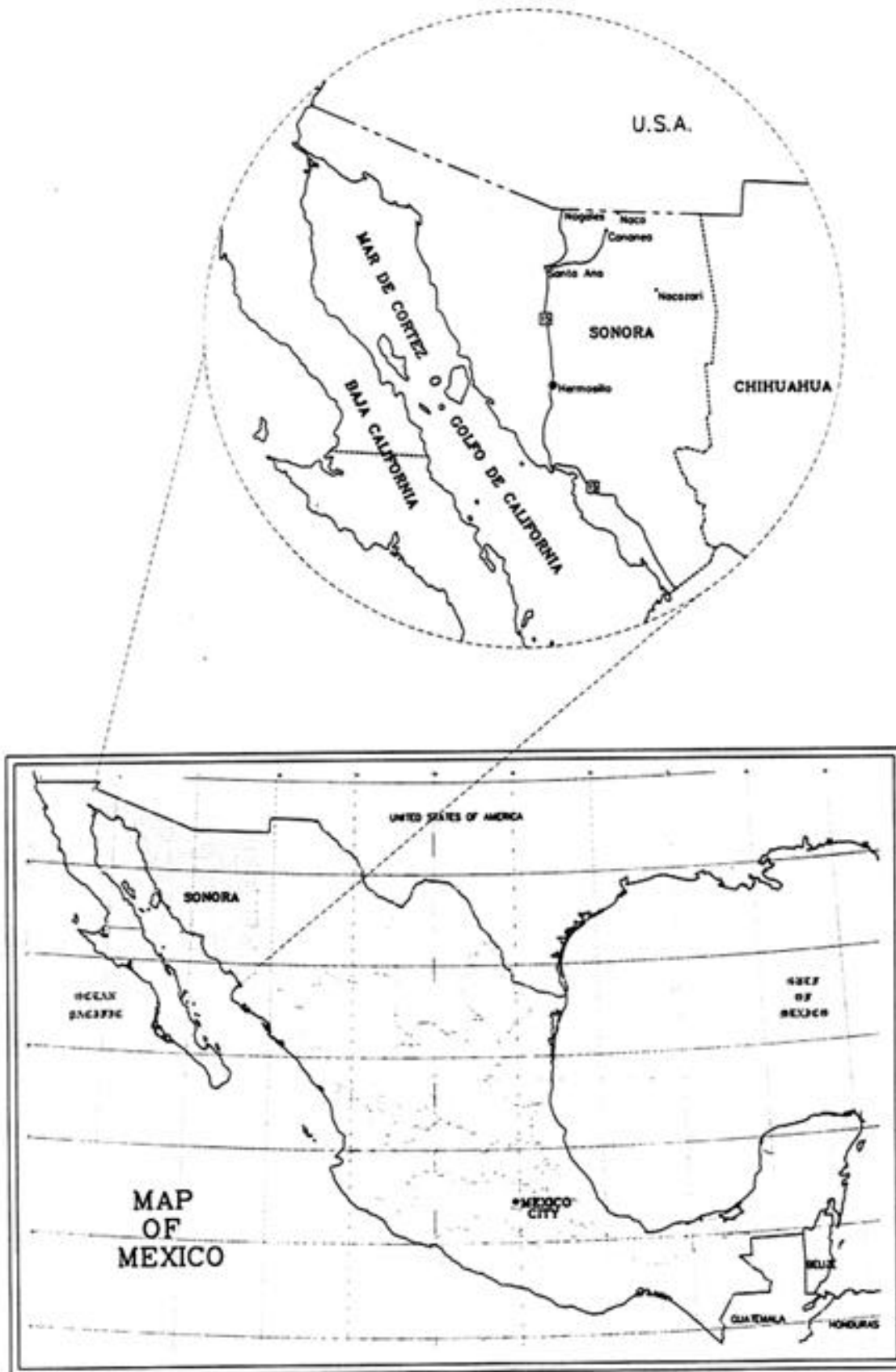
zona de la mesa: suelo con pendiente ligera, con estructura degradada en superficie, arenoso en la parte convexa con cobertura vegetal herbácea con predominio de *Bouteloua* (plantas perennes esencialmente):

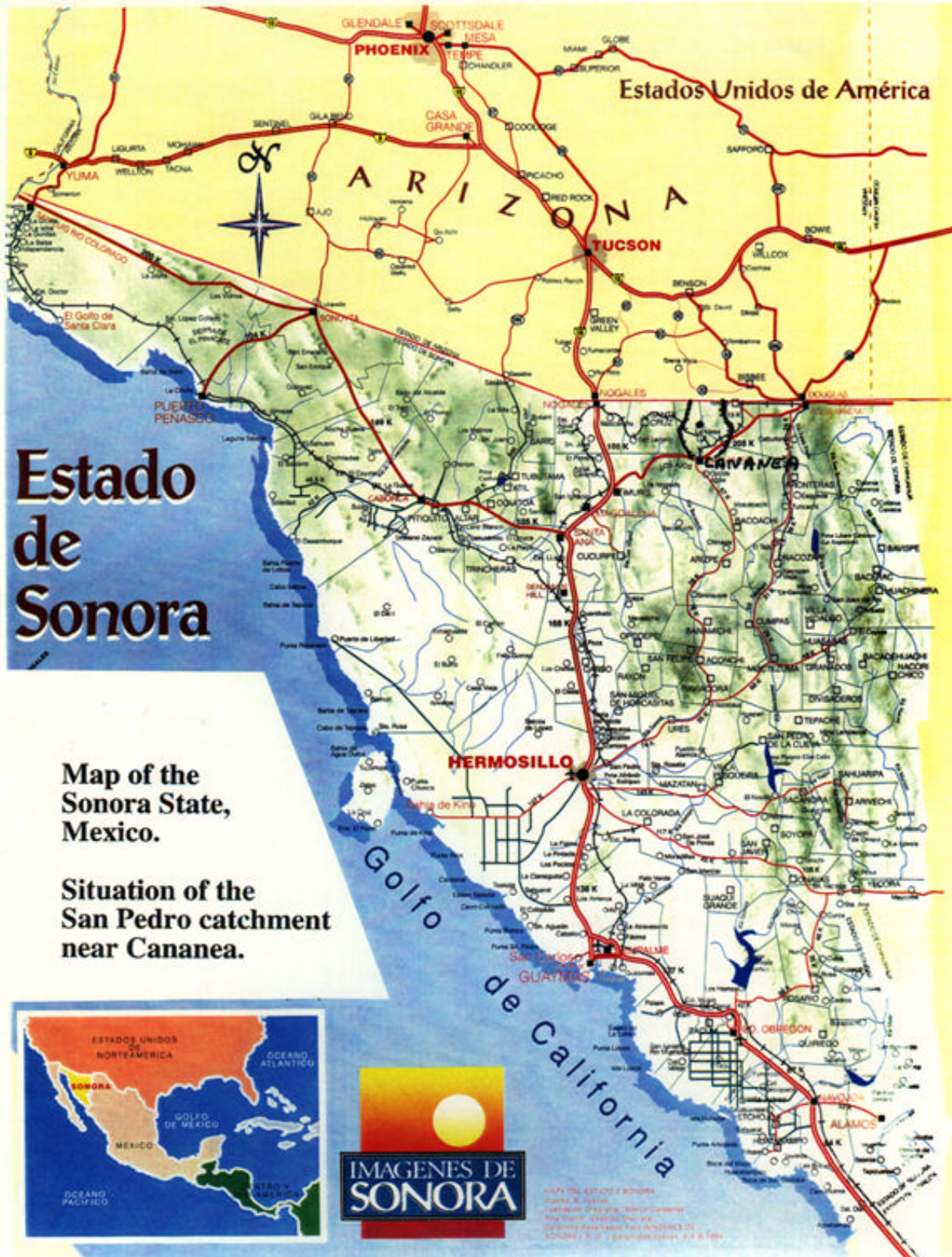
zona plana: suelo arenoso, rico en elementos finos en superficie, con cobertura vegetal herbácea más densa que en la mesa (plantas perennes y anuales):

zona que bordea el río: colector de aguas de escurrimiento, su amplitud es variable. Un gran número de álamos bordean el lecho y el banco es a menudo colonizado por mesquites, o, en su defecto, por cultivos de riego.

Los sistemas unitarios deben ser considerados como elementos interactivos en el interior del paisaje representado por el glacis montañoso.

En el sitio mesa, una estación metereológica completa de conformidad con las normas O.M.M.





Summary

The results of our study on ecosystem processes in the mountain plateau region of northeastern Sonora (Mexico) suggest that some climatic parameters such as rainfall characteristics, combined with long-term grazing of semiarid grasslands, prompt an increase in the spatiotemporal heterogeneity of water, vegetation and other soil resources. Soil water distributions throughout the area affect the soil surface properties (soil surface temperature, wind erosion), thus promoting the development of more adapted plants and inducing a negative effect on the growth phase in grassland ecosystems. The effects of these processes (desertization/desertification) on productive grassland have modified the general aspect of the catchment landscape. The general trend is an increase in bare areas in some parts, invasion of other types of grasses (annual), bushes and cacti, thus modifying the physiognomy of the landscape.

This study report highlights the overall trends based on nearly 1 year of weather parameters measurements, with emphasis on the summer intensive observation period involving microclimatic measurements on different types of grassland in the semiarid environment of northeastern Sonora.

Our aim is to inform Salsa project participants on the results of our 1996-1997 field study at the San Pedro catchment site (Mexico). The methods used to understand the different processes are presented along with some preliminary data.

1. INTRODUCTION

The interdisciplinary Semi-Arid Land Surface-Atmosphere program (SALSA) is aimed at obtaining responses to the following questions (Goodrich, 1994):

- => what are the consequences of climatic and human-induced change on the water balance and ecological diversity in the Upper San Pedro River basin?
- => what are the effects of such change at event, seasonal and interannual timescales?

The Upper San Pedro River basin is an ideal location (large plateau surrounded by mountains) to investigate:

1. the impact of anthropogenic change (e.g. overgrazing) with regards to desertification, sustainability and subsequent feedback effects on the regional hydrology and climate;
2. the effect of the summer season, under the influence of the "Mexican monsoon", on seasonal and interannual climate variability (desertization).

The Upper San Pedro River basin, near Cananea, in northeastern Sonora, has a large plateau that is of considerable interest for investigating poorly understood

land-atmosphere processes, as the area is a patchwork of different biomes with heterogeneous land-use patterns.

Responses to the main question were obtained by :

1. monitoring hydro-meteorological and ecological changes in order to determine seasonal and interannual variability;
2. investigating critical soil-vegetation-atmosphere exchange processes at different spatiotemporal scales.

The following strategy was adopted: low intensity long-term monitoring with intensive observations during the monsoon period at three biomes near Ej. Morelos in San Pedro basin. The programme included studies of meteorological parameters, micrometeorological measurements for radiation, water and energy fluxes, unsaturated zone soil moisture and vegetation biomass production within a nearly 5 km transect extending from the Huachuca foothills to the "mesa", integrating a variety of spatial scales. The transect is representative of the landscape in the San Pedro river catchment area.

The study is aimed at investigating temporal variability in surface radiation, water and energy exchanges, along with climatic forcing and surface conditions at three sites representative of the landscape in the San Pedro catchment. The following report highlights the field activities and some of the resulting datasets. In the first part, the catchment area is described, in addition to climate, vegetation and soil characteristics. In the second part, there is a detailed description of the instruments and methods used to monitor radiation, energy and water fluxes. Some illustrative results obtained during the 1996-1997 study period are presented in the last part.

It is still too early, at this data-processing stage, to draw any conclusions on critical desertization and desertification processes in this basin area. Complex interactions between forcing variables, such as solar radiation, precipitation and water vapour deficit, and the feedback effects of surface variables, such as soil wetness, soil temperature and vegetation gas exchange, have to be analysed and parameterized before assessing their role in the global climate system.

2. CHARACTERISTICS OF THE CATCHMENT AREA

2.1. Description of the catchment area and sites

(maps and satellite image)

The Mexican part of San Pedro valley is located in the semiarid mountainous northeastern region of Sonora, comprising the headwaters of the generally dry San Pedro river. Four mountains enclose the semiarid plateau, i.e. Los Ajos on the eastern side, San Jose more to the north, Mariquita/Elena on the western edge, and

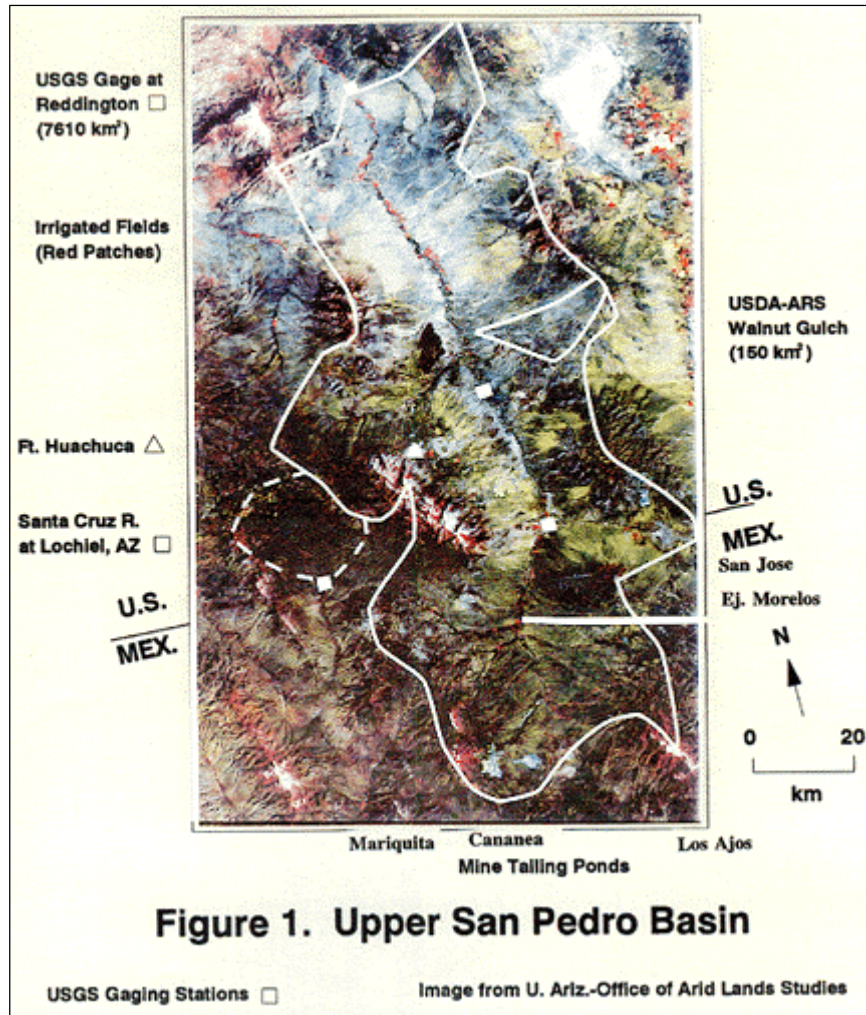
Huachuca mountain near the national border. The town of Cananea is on the southern limit of the plateau, with Naco on the northern Mexican limit of the catchment area, at the Mexico-USA border (see maps and satellite image).

The experimental study area presented here is located near Ej. Morelos. It includes a nearly 5 km transect located within a ranch at the Huachuca foothills. The slope of the terrain is 1-1.5%. The vegetation is characterized by a *Chihuahuan semidesert grassland*, and a typical mesquite grassland community on the upper part, with a variety of summer-active perennial grasses lower on the "mesa". In terms of the general physiognomy of this semidesert grassland, the native grasses generally have very short stems, with taller associated shrubby perennials.

2.2. Northeastern Sonora climate (region Cananea, Naco, Patos)

Mexico is influenced by large-scale wind currents within the InterTropical Convergence Zone (ITCZ), and the climatic conditions prevailing in the country are markedly affected by shifts in this zone. The ITCZ represents the meeting point of dry cold air from the north and humid tropical air from south/southwest (Gulf of California) and south-east (Gulf of Mexico). Disturbances develop between the two air masses and give rise to storms and rainfall. The "Mexican monsoon" corresponds to the uppermost edge of the ITCZ, affecting northern regions of Mexico, characterized by precipitation during a short period (3-4 months) in the summer, with the highest temperatures occurring just prior to the onset of rains.

In the northwestern region as Sonora state, summer deep convective activities are mostly associated with tropical disturbances moving northward from the southwestern coast of Mexico, from the Gulf of Cortez, and from the tropical eastern Pacific coast. This results in high-speed surface winds (10-15 m/s), heavy rains, sometimes with hail, and flash flooding.



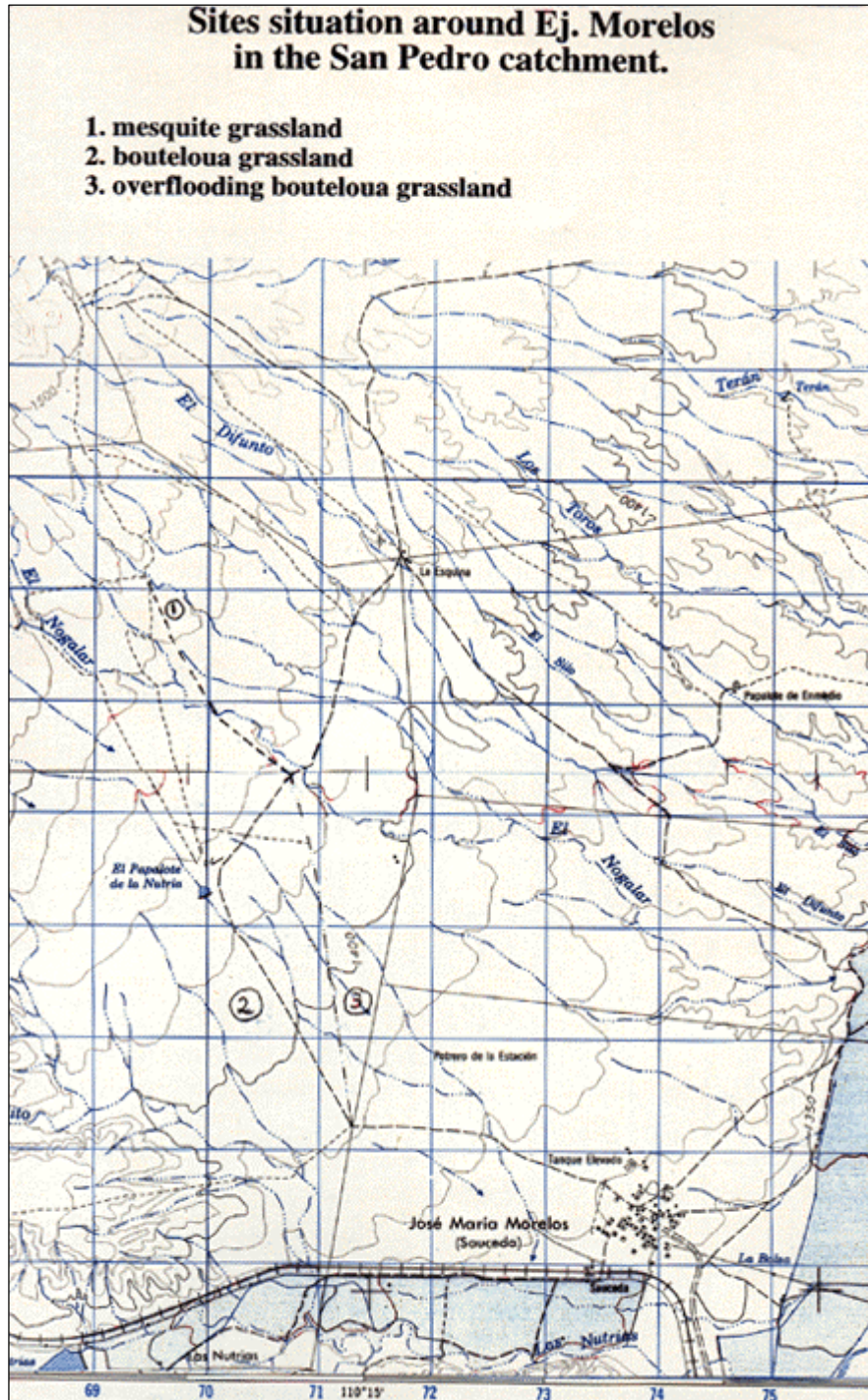


Fig 2.1. Evolution of the monthly mean precipitation and temperature at Naco (a) and Cananea (b) from 1962 to 1981.

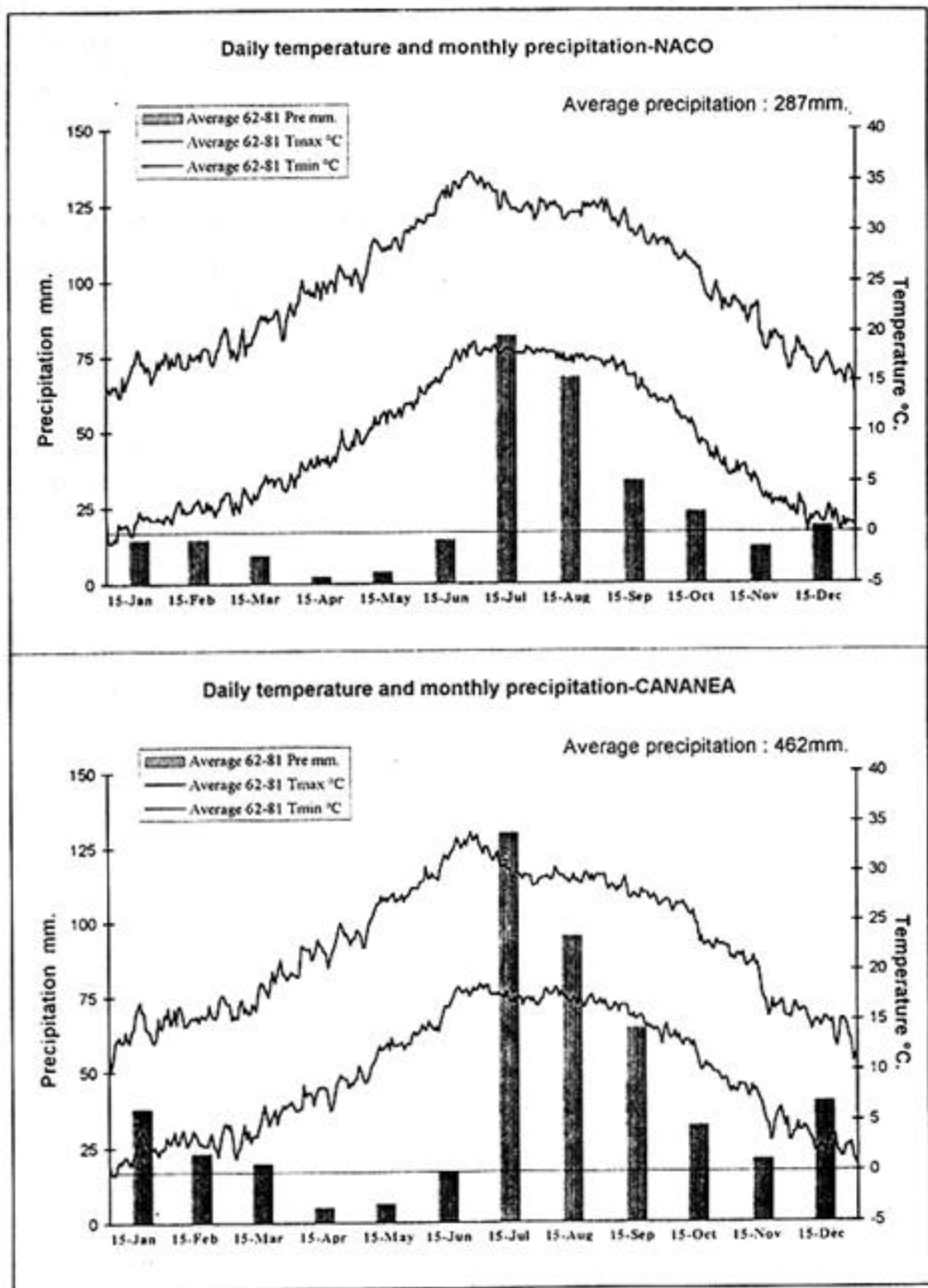
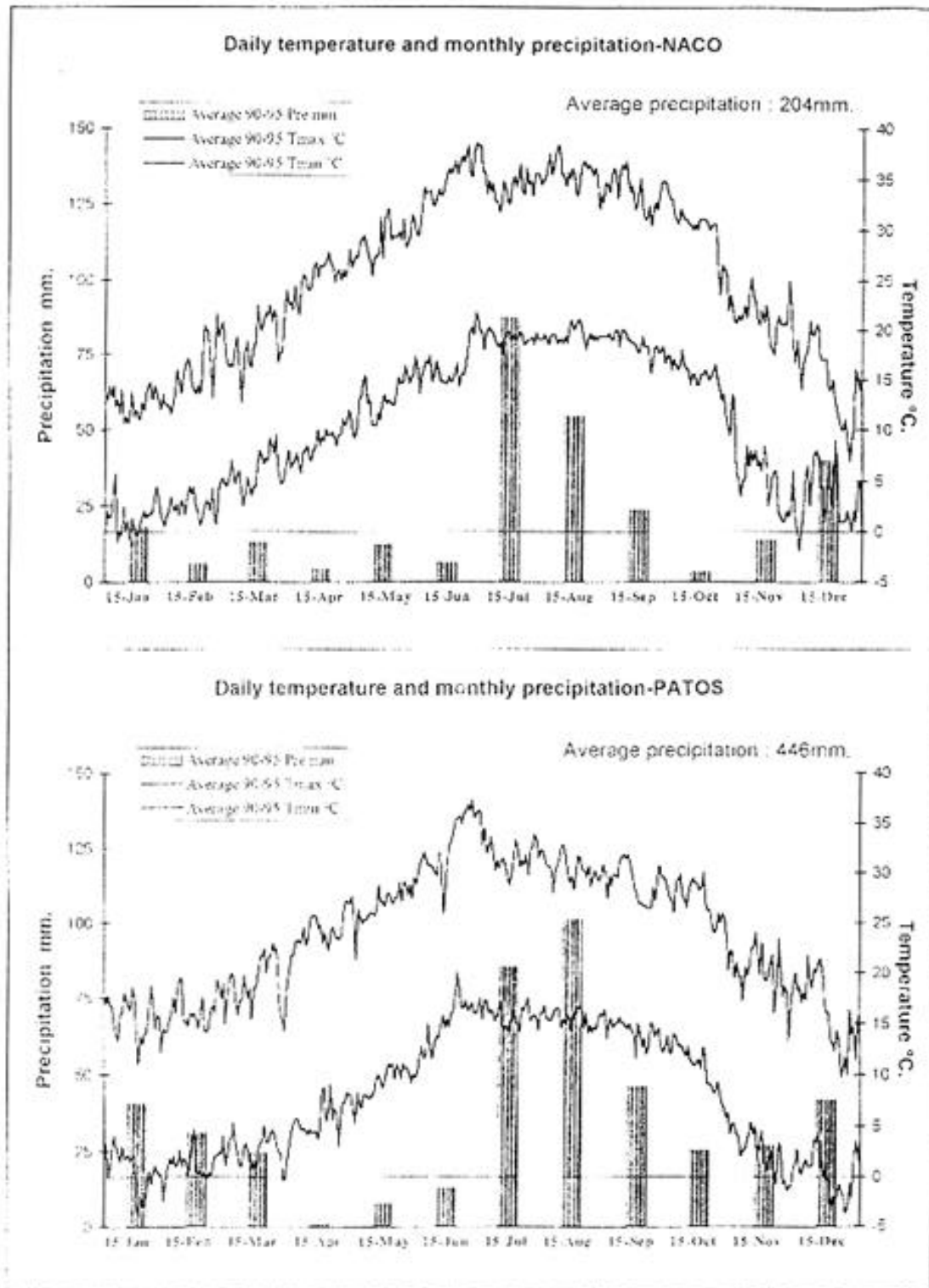


Fig 2.2. Evolution of the monthly mean precipitation and temperature at Naco (a) and Patos.(b) from 1990 to 1995.



There is also an orographic effect : the western slopes of the Sierra Madre Occidental receive more rainfall than the eastern slopes, which is related to the northeastward movement of humid air from the Gulf of California which has to rise up to be able to pass over the mountain ridge. The winter rainfall season is associated more with frontal storms, as cold air from the north meets warmer and wetter air from the southwest-west (Pacific Ocean and the Gulf).

The northeastern region of Sonora state has two distinct wet seasons. Precipitation is more or less abundant from July to September, and represents 60-70% of the total annual average rainfall (Fig. 2.1a for Naco and Fig. 2.1b for Cananea). Mean rainfall at Cananea is 462 mm/year (from 1962 to 1981) compared to 287 mm/year at Naco. Mean levels recorded at Naco and Patos for a recent 6-year period (1990-1995) are as follows: 204 mm/year at Naco and 446 mm/year at Patos (Fig. 2.2a for Naco and Fig. 2.2b for Patos). The differences could be explained by the topographical position of Naco, i.e. just northeast of San Jose mountain and by the altitude of Cananea (1680 m) and Patos (1550 m).

Rainfall has a marked effect, with a reduction of 3-5° C in maximum temperatures in July. During the November to March period, precipitation is caused by movement of the cold air front, as indicated by the fluctuations in maximum and minimum temperatures. The vegetation is dormant during this period. The mean evaporation rate is 2200-2500 mm/year. The rainfall distribution associated with the overall temperature trend is responsible for the semiarid climate in this region. The annual and summer rainfall departures, based on a mean for a 34-year period at Naco, are of considerable interest (Fig.2.3a,b). It shows the variability of the rainfall input year to year in this region. The eighties presents a wet trend, the nineties a drought one.

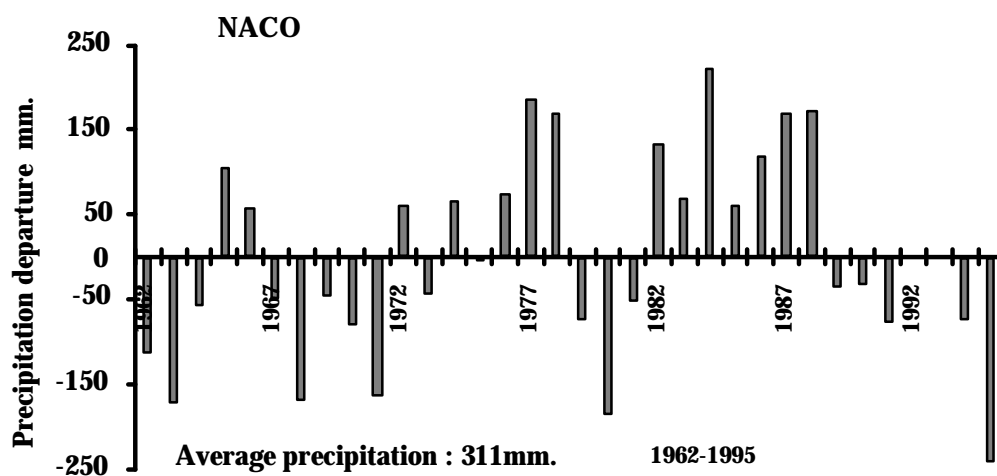


Fig : 2.3a . Annual rainfall departures using a mean of 311mm calculated from 1962-1995 at Naco.

The cumulative impact of these successive annual droughts has resulted in a decrease of the water table level. In fact, the water table is principally supply by the regular melting of the snow pack covering the mountains during the winter and the spring period. And in the nineties, the deficient of snowfall is well observed by the average minimum daily temperatures.

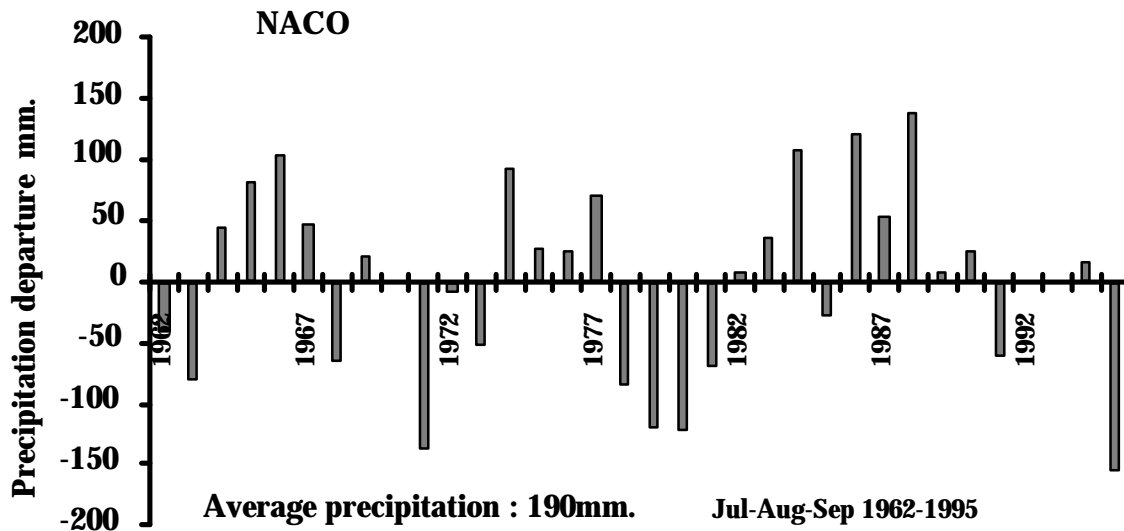


Fig : 2.3b. Summer rainfall departures based on a mean of 190mm calculated for the 1962-1995 period at Naco.

More interesting is the summer rainfall departures using the same period for Naco (fig.2.3b). It highlights the variability in precipitation during the summer in this semiarid region. There was also a wet trend through the 1980s, and considerable drought in the 1990s. The cumulative impact of these successive annual droughts in the 1990 was a decrease in grassland biomass production (personal communications of several ranchers). Although the general trend shows a decrease in total amounts of precipitation, spatio-temporal variability in rainfall events has to be taken into account, because this parameter is very important in this region as discussed later (§4.3).

2.3. Vegetation and soil surface conditions (photos)

Landform, topography, surface rockiness and soil type/origin have a direct effect on water availability through the redistribution of rainwater, i.e. the forcing factor for modelling the composition and structure of desert grasslands. In the San Pedro catchment, the landscape is gently undulating with low relief, and the physiognomy of the *Chihuahuan semidesert grassland* vegetation is as follows (see map):

- the lower limit of the semidesert grassland is at 1200-1400 m elevation, forming a mosaic landscape with desertscrub;

- the semidesert grassland plateau or "mesa" (1300-1700 m) offers some landscape diversity due to the vegetation distribution, which is linked to rainwater infiltration rates, soil characteristics and the history of livestock usage;
- the upper limit, with evergreen woodland, is at 1600-1900 m elevation depending on the mountainside area

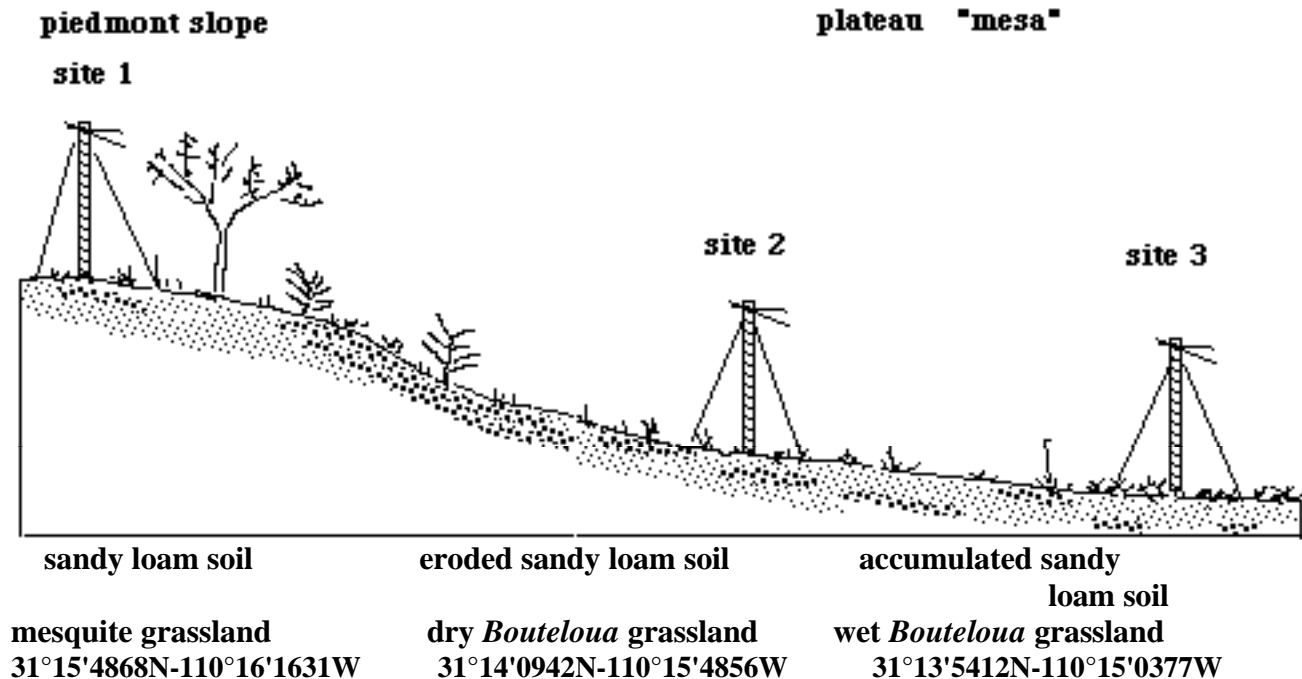


Illustration of the transect extending from the Huachuca mountain piedmont to the "mesa" showing the positions of the selected sites.

In the semidesert grassland ecosystem, there are summer active perennial bunch grasses, with the bases of the grass clumps separated by bare soil. The distance between bunches varies, and therefore the patchiness of the surface, depending on the extent of grazing and the rainfall level. As this distance increases, due to a combination of low summer rainfall distribution (desertization process) and overgrazing (desertification process), the bare soil surface increases (see photos). These factors alter the landscape physiognomy. The grassland is sparsely covered with C4 grasses, and C3 annual grasses to a lesser extent. The mean grass height is about 15-30 cm on eroded gravelly upland sites (called dry *Bouteloua* grassland), and 40-60 cm in collecting runoff areas (called wet *Bouteloua* grassland) where the edaphic conditions are not as limiting. Shrubs (mesquite and other acacias) have partially colonized some other parts. The piedmont slopes have coarser soils and are dominated by a disturbed grass canopy cover of *Bouteloua* sp. and *Aristida* sp., in association with bushes such as *Prosopis* gl.(?) trees and *Yucca*..

**Semidesert grassland ecosystem with dominant *Bouteloua sp.*
september 96**



**The same semidesert grassland ecosystem in september 97 :
the difference is due to less rainfalls and overgrazing.**



Mesquite grassland community near Morelos



**september 1996 : general view of the site,
biomass production covering the soil surface completely**



**september 1997 : sparse biomass production
due to water stress and partially overgrazed**

The following study sites were selected:

1. a mesquite grassland community near the foothills, i.e. a typical ecosystem at the edge of a semidesert grassland plateau (mesa);
2. the grassland plateau which offered some landscape diversity, with:
 - = a dry grassland site with *Bouteloua* cover, i.e. the dominant summer-active perennial grass of the "mesa" on gravelly upland locations,
 - = a wet grassland site (collecting runoff area) where summer-active perennial grasses associated with annual species grow in large patches, forming denser covers.

3. EXPERIMENTAL METHODS

3.1. Weather station at Morelos (31°14'0942N; 110°15'4856W; 1429m)

Routine, long-term monitoring of climate variables was undertaken at the Morelos meteorological station, which is located 35 km north of Cananea in the San Pedro catchment. Installation of an automated weather station necessitated specification of the variables to be measured and the measurement sensors, in compliance with the common standards set out by the World Meteorological Organization (WMO). The weather station is an integrated system even though the components were purchased separately. This enables better control of equipment quality and easy calibration verification. The weather station is installed at the dry *Bouteloua* grassland site (2), in the middle of the transect (see figure illustrating the weather station).

Table 3.1. : Weather parameters and sensors (photos)

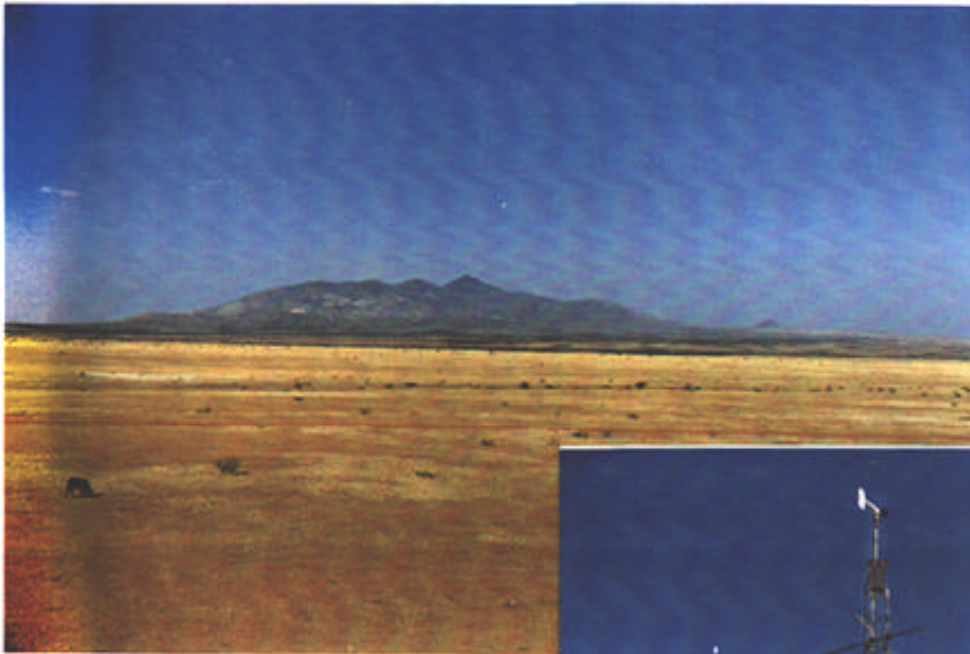
parameters	sensor	model	height (m)	sampling
solar radiation	pyranometer	Kipp&Zonen CM5	1.80	30 sec / 1h
PAR radiation	pyranometer	LI-COR Quantum	1.80	30 sec / 1h
reflected radiat.	pyranometer	Kipp&Zonen CM5	9.00	30 sec / 1h
precipitation	rain gauge tipping bucket	TE 525MM-L	0.60	60 sec / 20min
net radiation	net radiometer	Q6 REBS	9.00	30 sec / 1h
air temperature	thermistor	Vaisala HMP 35C	9 and 2.00	30 sec / 1h
relative humidity	sorption sensor	Vaisala HMP 35C	9.00 and 2.00	30 sec / 1h
wind speed and direction	propeller-vane anemometer	R.M. Young 5103	10.00	30 sec / 1h
wind speed	cup anemometer	Vector - UK	2.00	30 sec / 1h
soil temperature	thermocouple		-0.02	30 sec / 1h
surface soil temperature	infraredthermo-radiometer	Everest 4000	9.00	30 sec / 1h
acquisition power supply protection box	data logger solar panel + car battery	CR10 X + AM416	in a screen	

The data logger was programmed to sample most of the parameters every 30 s, with 1 h mean reports, except for the raingauge (integration every 20 min). It operated automatically 24 h/day. Most of the sensors were fitted on a guyed galvanized tower, only two pyranometers and a cup anemoter were installed separately (Table 1.). The Young propeller was installed on the top of a 10 m tower.

The data were collected regularly from the outset of the study, beginning in September 1996 for the climatic variables and on September 18, 1996 for some of the vegetated surface radiation budget components (schedule Table 4.1.).

Estado de avance de la disposicion de los dispositivos de medicion para la evaluacion y la caracterizacion del proceso de evolucion del estado de la superficie en zona semi-arida. - MONTENY, B.A. (junio 97) en la cuenca del San Pedro, cerca del Ej. Morelos (a 30km de Cananea)

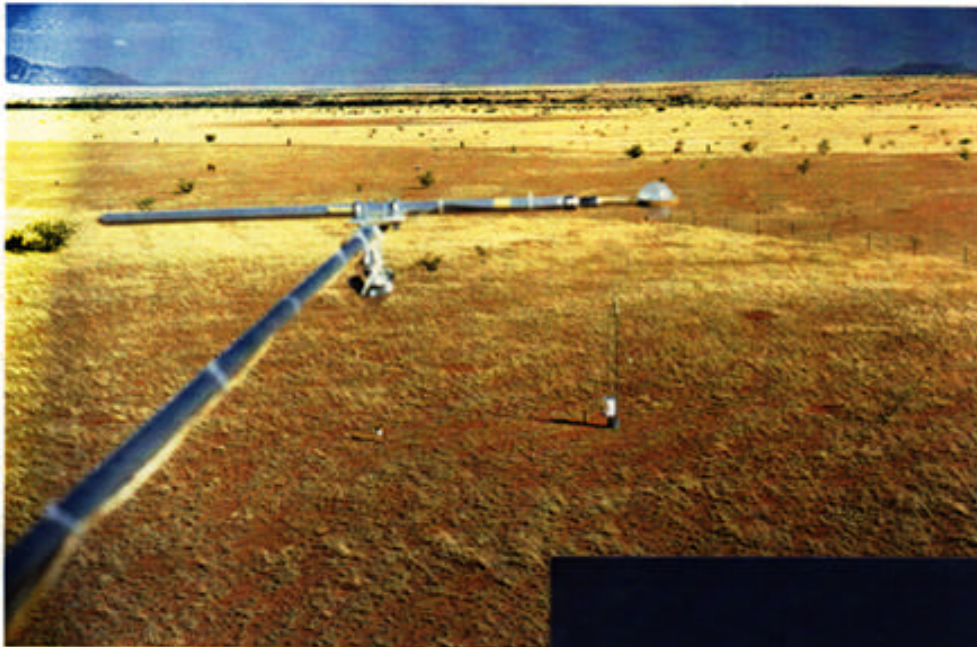
Vista general de la estructura herbacea de sitio 2.



Dispositivo de medicion de los parametros climaticos de la region en niveles de 2 y 10 metros.

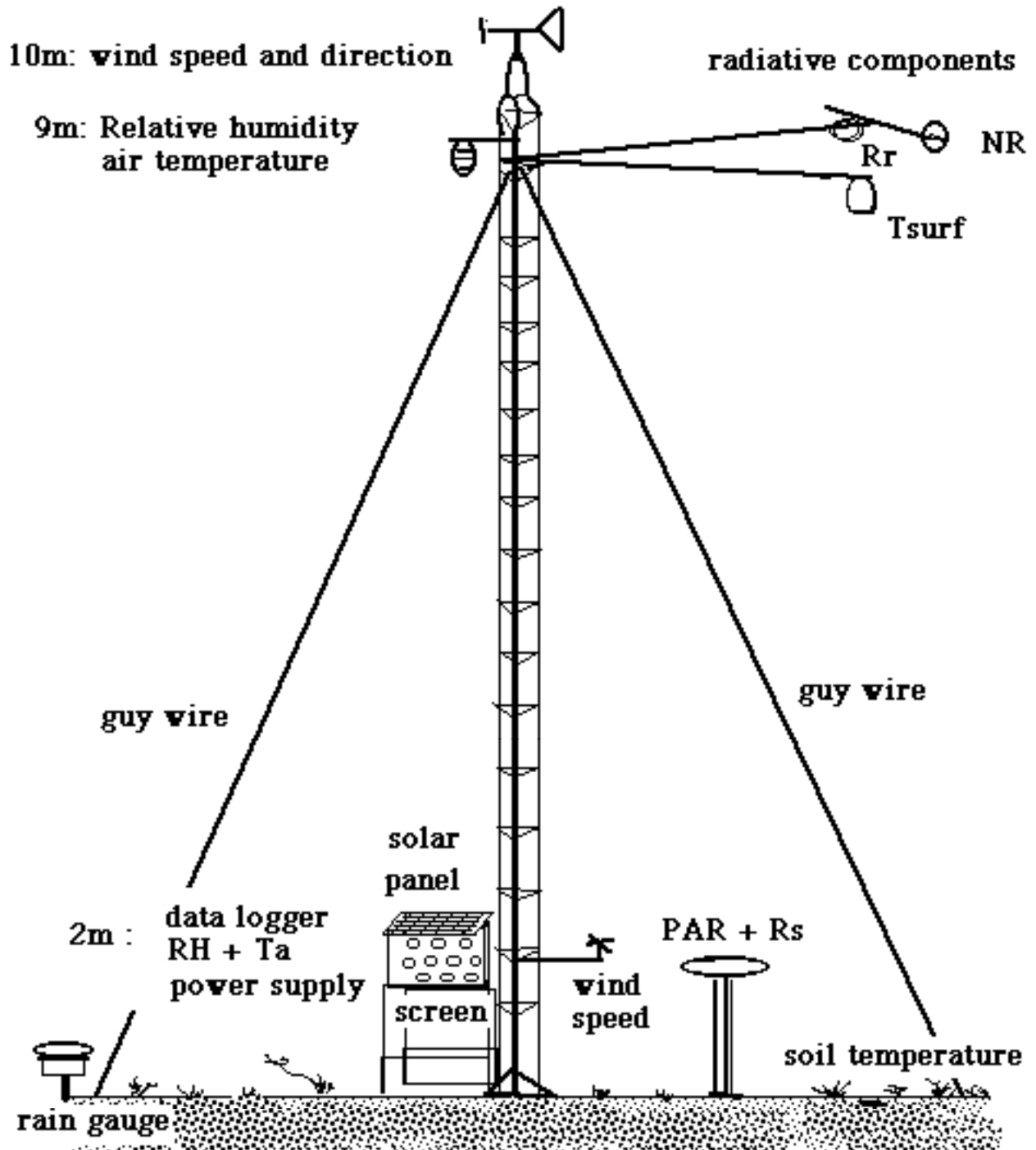


Vista aerea del sitio 2 de "estructura herbacea" y la disposicion de mediciones microclimatologicas para la evaluacion del balance energetico.



Vista para mostrar la disposicion de los equipos para la evaluacion del balance de radiacion, temperatura y humedad del aire y medicion de la velocidad y direccion de las masas de aire.





radiative components : Rr : reflected radiation; NR : net radiation
 Tsurf : soil surface temperature
 PAR : photosynthetic active radiation
 Rs : solar radiation

air mass characteristics : speed and wind direction
 at 2 levels humidity and temperature

precipitation; subsoil temperature (-0.02m)

3.2. Radiation budget and available energy $R_n - G$ (photos)

Various radiation budget components were measured continuously from different biomes in order to efficiently assess the effects of surface properties on available energy. The radiation budget of the sparsely vegetated surface is:

$$R_n = R_s - R_r + \epsilon R_a - \epsilon \sigma T_s^4 \quad (\text{Wm}^{-2}) \quad (1)$$

where R_n : the net radiation flux density; R_s : the incoming shortwave solar radiation, R_r : the reflected shortwave radiation ($=aR_s$) with a : albedo; ϵR_a : the incoming long wave radiation and $\epsilon \sigma T_s^4$: the emitted longwave radiation with $\sigma =$ Stefan-Boltzmann constant, ϵ the emissivity assumed to be equal to 0,93 for dry bare soil and 0,97 for the vegetated area and T_s : the surface temperature K° .

Incoming solar radiation R_s and the photosynthetically active radiation PAR (400 to 720nm) of the incoming solar radiation were measured with a Kipp CM5 pyranometer (Kipp&Zonen, Delft, Netherlands), calibrated against an Eppley radiometer, and a quantum sensor (Campbell Scientific, Shepshed, UK) respectively. These radiation data are recorded continuously at the meteorological station.

Before the intensive observation field study, five net radiometer sensors of the same make (REBS Q6) were recalibrated over a large homogeneous area and positioned 2 m above the soil surface. The aim was to avoid differences between net radiometers when comparing data from different types of surfaces.

The main radiative characteristics of the soil-vegetation surface are reflected R_r and emitted radiation $\epsilon \sigma T_s$. But the heterogeneity of the sparsely vegetated surfaces has to be taken into account when making measurements and interpreting the data. The downward-facing radiometers respond to a cosine-weighted average of incident fluxes upon the hemispherical windshield. To evaluate the effect of irregular spatial distributions of perennial bunch grasses, four net radiometers R_n (Radiation Energy Balance System, REBS Q6) were used above the sparse vegetated area, at 3 m height, to evaluate the impact of variability of surface characteristics on net radiation. The calculated average corresponds to a mean for 2, 3 and 4 sensors, and smoothes out the fluctuations. The results show that a minimum of two net radiometers are necessary at this height to improve radiation balance values for sparsely vegetated surfaces (Fig. 3.1.). However, we could only use one because of financial constraints, which was positioned higher. At all sites, the net radiometer was fitted on a 3 m arm positioned 9 m above the flux station towers (photo). Net radiation values at 9 m gives an areal average, integrating the heterogeneity of the surface, and corresponding to a mean of three other net

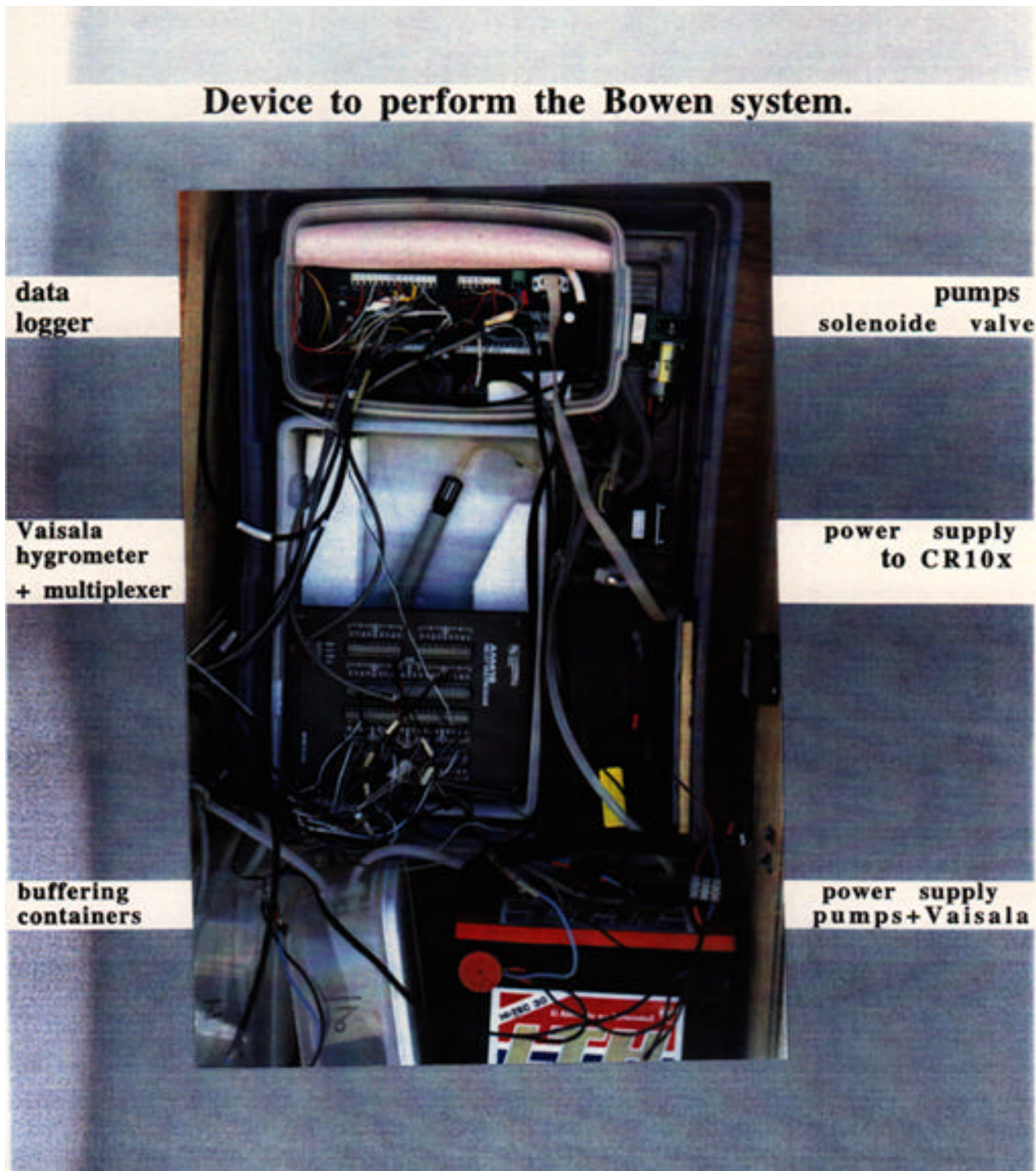
radiometers positioned at 3 m. These aerial measurements are better spatial integrators, representing an average areal value for the radiation budget of the vegetated surface equivalent, approximated at 800 m², as reflected, emitted and net radiations can be measured within a 90° view angle. The pyranometers were installed high enough to integrate cosine-weighted views of bare soil and vegetation in the same proportions observed at the sites.

Sitio 1. : Vista general del sitio de arboles con estructura herbacea cerca del Monte Huachuca de la cuenca del rio San Pedro (35km de Cananea).



Disposicion general para medir las diferentes características del balance de radiacion y balance de energia.





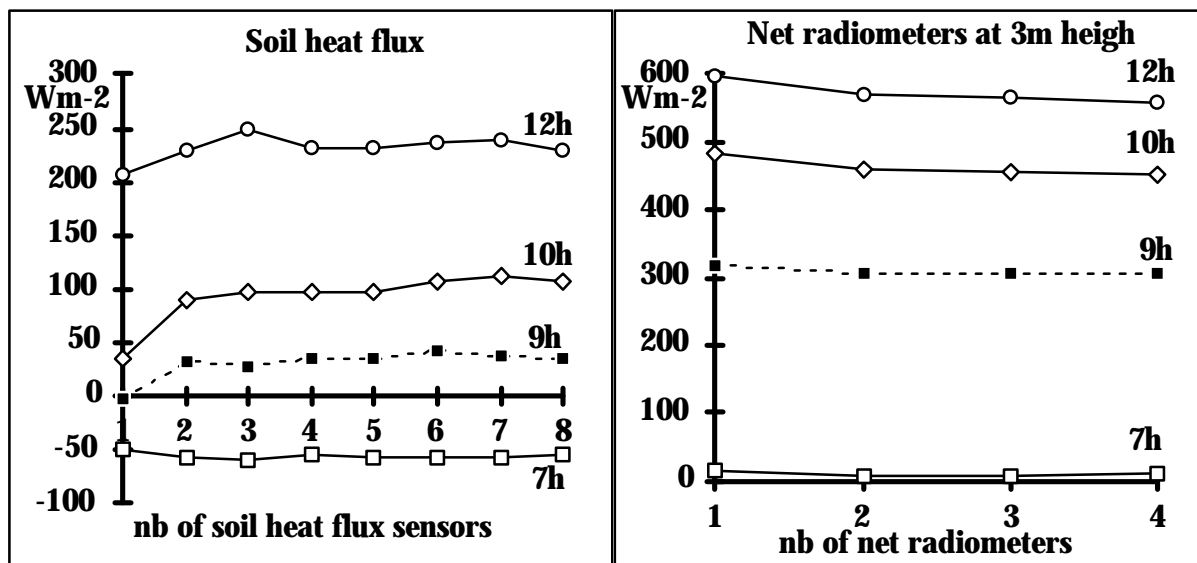


Fig. 3.1. : Number of sensors required to accurately evaluate soil heat flux and net radiation over a sparsely vegetated surface.

For the same reason, short-wave reflected solar radiation R_r and emitted long-wave radiation $\epsilon\sigma T_s^4$ were measured at the same height above the studied surfaces. We used an inverted pyranometer (Kipp & Zonen CM5) to measure short-wave reflected solar radiation R_r , and the surface temperature was measured with a chopped thermoradiometer (model 4000, Everest Interscience, Tucson, USA) at nadir position to evaluate emitted long-wave radiation $\epsilon\sigma T_s^4$. The net radiometer R_n (Radiation Energy Balance System, REBS Q6) was mounted horizontally. R_n and R_s were checked regularly to verify the consistency of the measurements. The net radiometers used in the field were calibrated outdoors against a factory calibrated net radiometer.

Soil heat flux of a patchy surface may represent 30-45% of the net radiation, especially when the soil is dry. This component has to be measured carefully to obtain an accurate evaluation of the surface energy budget. However, soil heat fluxes are difficult to measure in sparse vegetation as the source area viewed by the sensor (0.013 m^2) is smaller than for the other sensors, and because vegetation shades the soil surface. To accurately evaluate the mean soil heat flux while avoiding distortion of the soil heat flux pattern, eight soil heat plates were buried at 0.02 m depth, in a horizontal line, in an area viewed by the net radiometers. A measurement was obtained every 10 s, with averages calculated every 10 min. Figure 3.1. presents, for different hours of the same day, mean soil heat flux values with one, two or more soil heat plates. The heat stored within the first 2 cm was disregarded. After 4 months of measuring net radiation and soil heat fluxes in

different climatic conditions, we came to the conclusion that at least four plates have to be buried to accurately estimate of the areal average soil heat flux for this sparsely vegetated area.

3.4. Precipitation / soil moisture availability

Summer rainfall accounted for 60-70% of the annual precipitation. It is the most important forcing input variable in the vegetation cycle for all realistic climatic models. Rainfall quantity and intensity were accurately measured to simulate changes in soil surface properties as well as surface boundary conditions. We considered that this was the main physical factor affecting summer grass production from July to September.

At each site, an automatic tipping bucket rain gauge station was installed and connected to a solid-state data logger to measure the quantity, intensity, duration and times of rainfall events. Both the temporal and spatial distributions of rainfall events were considered: nine other total recording rain gauges were positioned at different points along the transect from the foothills to the mesa in order to determine the spatial distributions of precipitation (see § 3.5.).

Soil moisture affects the energy budget through the evaporation rate. The following measurements were obtained to assess soil water availability and variations with the aim of evaluating the water budget at each site:

- * gravimetric sampling profiles to calculate gravimetric and volumetric soil moisture contents at different locations. They were weighed in the field, dried in an oven at 95°C for 2 days and weighed again to calculate the soil water content (% and vol. in mm). In the flooding zone, samples were regularly obtained below the grass roots;
- * profile measurements of soil water potential ψ by automatic sampling techniques using soil moisture blocks with blocking capacitors (Campbell Scientific Inc. sensors), connected to a multiplexer AM416 linked to a solid-state data logger. Two sets were installed at each site at -3, -5, -10, -20 cm depth, with one set installed at -30, -40, -50 cm depth. The top layer was of the most interest because of large area of bare soil, i.e. 80-85% of the surface. This layer offers high resistance to water vapour flow during the soil evaporation process. Due to the low water-holding capacity at the gravelly upland sites, a data logger was used to obtain continuous measurements in order to investigate short-term soil water potential dynamics. The soil water potential values are averages at each level measured every 20 min. These water potentials will be related to the soil water content, and the curve will help us evaluate changes in soil water dynamics during interstorm periods.

3.5. Scale variability

There is no available information on spatial rainfall distributions throughout the area. It is well known that rainfall events are highly scattered in semiarid areas. To determine rainfall variability throughout the study area, nine total rainfall recording gauges (direct reading after each event) were installed within a transect extending from the piedmont to the "mesa" plateau 5 km away.

Concerning soil moisture contents at grassland sites, the position and stage of development of bunches of *Bouteloua* grass on the soil surface, the crusting of the soil surface and the microtopography may affect infiltration rates and surface runoff. The quantity of infiltrated water can vary between sampling points, and this has to be taken into account when calculating the site water budget. The soil was regularly sampled at 0-5, 5-10, 10-20 cm, depending on the depth of *Bouteloua* grass roots, and sometimes 20-30 cm to 30-40 cm deeper after rainfall events, at the three different sites. At site 2, we measured also the soil water content inside the fence area (no grazing) and outside (grazing) to evaluate the impact of bunch grasses on infiltration rates and on the soil water content.

At the collecting runoff area (wet grassland site 3) where the vegetation is more dense, soil moisture profiles were sampled at different places due to soil/vegetation heterogeneity (photo). The sampling depths were 0-5, 5-10, 10-20, 20-30 cm depending on the root depths, and sometimes 30-40, 40-50 cm depending on the soil moisture content. The mean soil moisture content at this site gave us a global qualitative (but not quantitative) indication concerning the extent of surface runoff.

At the mesquite site (1), we used the same sampling technique but the periods between data collection varied because there was less rainfall.

Grassland production was measured in the fall using the following sampling technique: areal dry matter production was evaluated from the weight of biomass collected at 3 or 4 plots (1 m²) at each site.

The spatial distribution of the following variables was also assessed for the entire area : surface albedos and temperatures, net radiation, soil heat fluxes at -2 cm and soil temperatures, soil water potential at different depths and convective exchange rates between the surface and the atmosphere.

3.6. Soil-vegetation-atmosphere interactions

As convective fluxes of heat and moisture to the atmosphere are highly dependent on surface conditions, the measurements were obtained throughout the "homogeneous" terrain with large fetch at the three selected sites.

Micrometeorological methods are well suited for measuring vertical evaporation flux over land surfaces without altering the surface environmental conditions. The Bowen ratio/energy balance (BREB) was used to measure evaporation and sensible fluxes over vegetated surfaces, associated with the σT method to calculate the sensible heat flux (H). The results will be used to confirm the sensible heat values obtained by the Bowen ratio method.

3.6.1. Measurements of the energy budget components

The energy budget of a vegetated surface, when ignoring small storage terms, can be written for steady state conditions as :

$$\mathbf{Rn - G = \lambda E + H} \quad (\mathbf{Wm^{-2}}) \quad (2)$$

where Rn : the net radiation flux density; G : the soil heat flux density ; Rn-G : the available energy at the surface which is used by turbulent transfer to the atmosphere as latent heat flux density λE (with E the evaporation and λ the latent heat of vaporization) and sensible heat flux density H.

For many years, Bowen ratio technique has been used in conjunction with energy balance to assess areal evaporation. By assuming steady state conditions and horizontal homogeneity and assuming that the aerodynamic turbulent resistances of sensible and latent heat flux are equal near the surface, the Bowen ratio, $\beta = H/\lambda E$, can be derived from vertical gradient of air temperature, dT, and water vapour pressure, de, in the atmosphere :

$$\mathbf{\beta = (\rho_a C_p / \varepsilon \lambda) (dT/de) = \gamma * (dT/de)} \quad (3)$$

with ρ_a : the density of dry air, C_p : specific heat of air at constant pressure, ε : ratio of molecular weights of water vapour and air, λ : latent heat of vaporization

Considering that the available energy Rn-G can be measured directly and carefully, sensible heat and latent heat fluxes can be determined from the energy budget (Equation 2) :

$$\mathbf{\lambda E = (Rn - G) / (1 + \beta)} \quad (\mathbf{Wm^{-2}}) \quad (4)$$

$$\mathbf{H = \beta * (Rn - G) / (1 + \beta)} \quad (\mathbf{Wm^{-2}}) \quad (5)$$

The evaporative fraction $\lambda E / (R_n - G)$ characterizes energy partitioning over land surfaces. Three flux stations were installed in the transect: one in a gravelly upland area with short perennial *dry Bouteloua* grass cover, the second station is in a more humid area with denser grass vegetation (*Bouteloua*, *Hillaria* dominant with annual plants) and the third station is over the mesquite grassland ecosystem in the upper part of the transect (see § 2.3.).

The aim was :

1. to evaluate the importance of the evaporation rates in the three ecosystems present in the area in relation to rainwater input and the possibility to aggregating the different energy budget components for a large area within the catchment.
2. to assess ecological modifications due to rainfall variability in order to determine seasonal changes;
3. to investigate critical processes which modified soil-vegetation-atmosphere exchanges progressively over time and thus at different spatial scales.

Latent and sensible heat fluxes were calculated from a gradient of mean temperature and water vapour pressure values at the same levels (*what is at the same level?*) through the energy budget/Bowen ratio method. In the two grassland areas, the sampling height was 0.40 m and 1.4 m, and sampling was done 4 m and 9 m above the canopy in the mesquite grass area. Temperatures were measured with shielded copper-constantan thermocouples and water vapour pressure was measured with a humidity sensor (Vaisala HMP35A, Vaisala Inc, Helsinki, Finland). Air was sampled alternately with two pumps (ASF, Puchheim, Germany) at both levels. It passed through porous (40 μm) ceramic dust filters and was drawn through a tygon line into two mixing reservoirs. From there, the air passed through a three-way solenoid valve, which was activated every 150 s by a signal from the data logger. It diverted the flow through the capacitive hygrometer sensor. The sensor was placed inside a measurement chamber of about 1 cm^3 . For the purposes of stabilization, measurements obtained during the first 40 s following inversion were excluded, and then the air temperature and humidity in the chamber were measured every 10 s and immediately converted into vapour pressure by a CR10X data logger (Campbell Scientific, Shepshed, UK). These values at both levels were then averaged for 20 min intervals. The two pumps, two 2 liter buffering containers, the solenoid valve, hygrometer and data acquisition system (CR10X + AM416) were protected in polyethylene boxes from dust and rainwater (see photo). All of these boxes as well as the power supply were placed in a wooden box attached on the tower, i.e. to protect these units against lightning, which can destroy the whole electronic system.

3.6.2. Independent Sensible heat flux evaluation.

Sensible heat flux can be evaluated by the temperature fluctuation method, a simple measurement of the standard deviation of the temperature, σ_T . It is based on the similarity theory of Monin-Obukhov and should only be applied in unstable atmospheric conditions. The sensible heat flux is calculated through the following equation :

$$H = \rho_a C_p \{(\sigma_T/C)^3 * (k*(z-d)*g / (T+273.2))\}^{1/2}. \quad (6)$$

with ρ_a : air density ; C_p : specific heat of air at constant pressure; T : mean air temperature at height h ; k : von Karman constant : 0,4; g : the acceleration of gravity; z : the level at which σ_T is measured; d : displacement height; C constant (0,95) .

The measurements are valid only in unstable conditions, after sunrise and before sunset. Values are obtained with fine-wire thermocouples constantan-copper, fixed on arms extending 2,5m from the tower, 1,4m above the vegetation surface. Datas were recorded on a data logger CR10X over 20 minutes intervals.

4. PRELIMINARY RESULTS

Quality control of the data

Generally, missing or wrong values were derived from linear relationships obtained between two instruments as incoming solar radiation and net radiation or photosynthetic active radiation ; soil surface temperature measured by an infrared thermo-radiometer and by thermocouples. The destruction of the net radiometer dome by birds or by hail, the presence of spiderwebs or bird feces on the dome, as well as condensation of water vapour inside the instruments sometimes led to incoherent net and solar radiation values. The cup anemometer could also malfunction due to the presence of spiderwebs or sand which affect its rotation.

Air temperature measured with thermocouples and water vapour pressure measured with the Vaisala at different sites at 1.4 and 2.0 m were checked to ensure reasonably comparable results. No noticeable calibration drifts were noted with the Vaisala humidity sensors over the 4-month study period. Values obtained during and just after rainfall can be disregarded for calculation of the radiation and energy budget components.

For the flux calculations, the temperature gradient inversion at sunrise and sunset affected the Bowen ratio values and thus partitioning of available energy into latent and sensible heat. The values were interpolated from preceding and subsequent values. When no actual data were available, the missing integrated 20 min data for temperature or water vapour pressure was also interpolated for the energy flux calculation. When the data were beyond the instrumental accuracy range, as was the case for the between-level difference in water vapour pressure for the Bowen ratio system, they were ignored and no fluxes were calculated. Missing data was due to instrument failures (air pump, multiplexer...), system limitations (power supply from batteries, insufficient memory), or the fact that we were sometimes unable to go to the field. A schedule chart presents the measurements obtained at different sites and the timing of each experimental task.

Table 4.1 : Schedule of measurements at different sites.

site	parameters	start	stop	comments
climatic station	P,Rs,PAR, Ta,HR,V+D, 2and10m	4.09.96		hourly and daily values
mesquite grassland ecosystem	P, Rn, Rr, Tsur, Ta, G HR, Tso+ ψ_{so} at depth; soil water content BREB	13.08.97 16.07.97 22.07.97 30.08.97	25.11.97* 25.11.97* 14.10.97 06.11.97	components of radiation, water + energy budgets: 20min. values to low evaporation
dry bouteloua grassland ecosystem	+ Rn -G + Rn,Rr, Tsur, Ta, HR, Tso + ψ_{so} at depth + soil water content BREB σT	09.96 04.97 04.97 15.07.97 08.05.97 24.06.97 22.01.97	25.11.97* 25.11.97* 25.11.97* 07.11.97 23.10.97 25.11.97*	available energy components of radiation, water + energy budgets: 20min. values not continuous
wet grassland ecosystem (runoff collector area)	P,Rn,Rr, Tsur, Ta, G HR, Tso+ ψ_{so} at depth soil water content BREB σT	16.07.97 27.07.97 20.07.97 22.07.97 22.07.97	25.11.97* 25.11.97* 07.11.97* 23.10.97* 25.11.97*	components of radiation, water + energy budgets: 20min. values
rainfall stations	rain distribution over the study area	11.06.97	15.10.97	daily values

* some scientific sensors have to be bring back to the mexican custom office.

BREB : Bowen ratio energy budget

σT : standard deviation of the air temperature

4.1. Morelos site climatic characteristics

The weather parameters measured by the automatic station will be used as modelling components for this study, and to obtain complementary information on near surface climatic conditions prevailing in the northeastern region of Sonora, Mexico. Very little data from the climatic station is missing (see § 4.1.). Day-to-day variability in climatic parameters, such as temperature, water vapour pressure or solar radiation, may conceal gradual trends from one type of regime to another with the movement of cold/dry or warm/humid air fronts. The effects of short-term irregularities can be eliminated by a statistical technique, i.e. moving averages. The method involves calculating mean values for successive overlapping periods (5-day periods here). This smooths out the very short-term trends. Figures 4.1. and 4.2. present the overall variations in climatic conditions during 1996-1997 as well as conditions prevailing during the intensive observation period (I.O.P.).

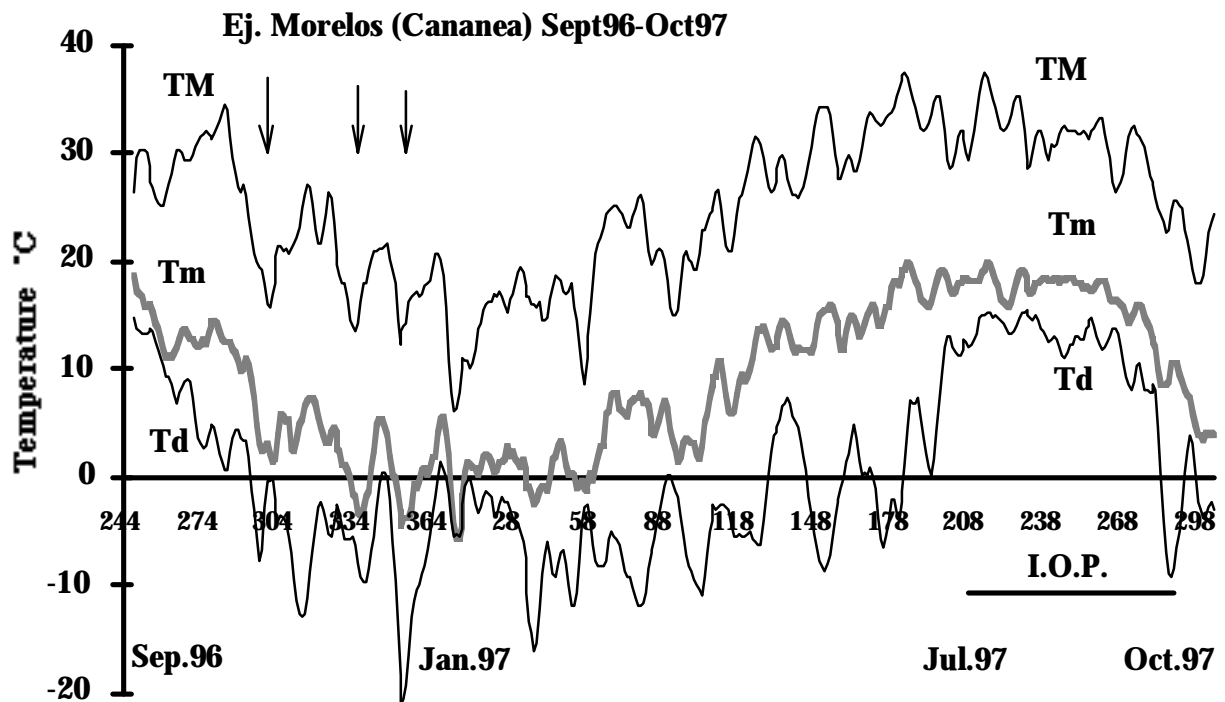


Fig 4.1. : Evolution of the maximum TM, minimum Tm and dew point Td temperatures at Morelos from September 1996 until October 1997.

The sinusoidal trend for maximum and minimum temperatures reflected the general influence of solar radiation or, more specifically, the balance between absorbed solar radiation and the effective outgoing radiation during the year. Solar radiation is minimal during the winter period and maximum in summer due to the Earth's rotation. The marked maximum-minimum temperature fluctuations were due

alternate cold dry and warm humid air fronts. Cold dry fronts appeared from October 1996 until April 1997. They came from the north/northwest and were associated with a southward shift of polar air outbursts over the United States. Drastic decreases in air temperatures were observed, associated with clear blue skies. Increased air temperatures were due to airflows of more warm humid air coming from the southwest that lost part of their moisture over the mountains. The temperatures were above seasonal normal levels, as observed during the winter months.

Dew temperature (Td) monitors spells of cold/warm air and was generally 5-10° C lower than minimal temperatures, except when it rained. During the summer period, from July until the end of September 1997, dew point temperatures increased from -10/-7° C to approximately +15°/+17° C. At this time, the northeastern region of Sonora was under the influence of moist southwesterly air masses. Summer rainfall comes with the advancing "Mexican monsoon". Dew temperature (Td) was almost equal to the minimum temperatures, which means that fog could cover the catchment area, with dew on plant leaves in the early morning. This year, the rainy season began mid-July and finished mid-October. Rainfall peaked in August and cloud cover reduced incident solar radiation.

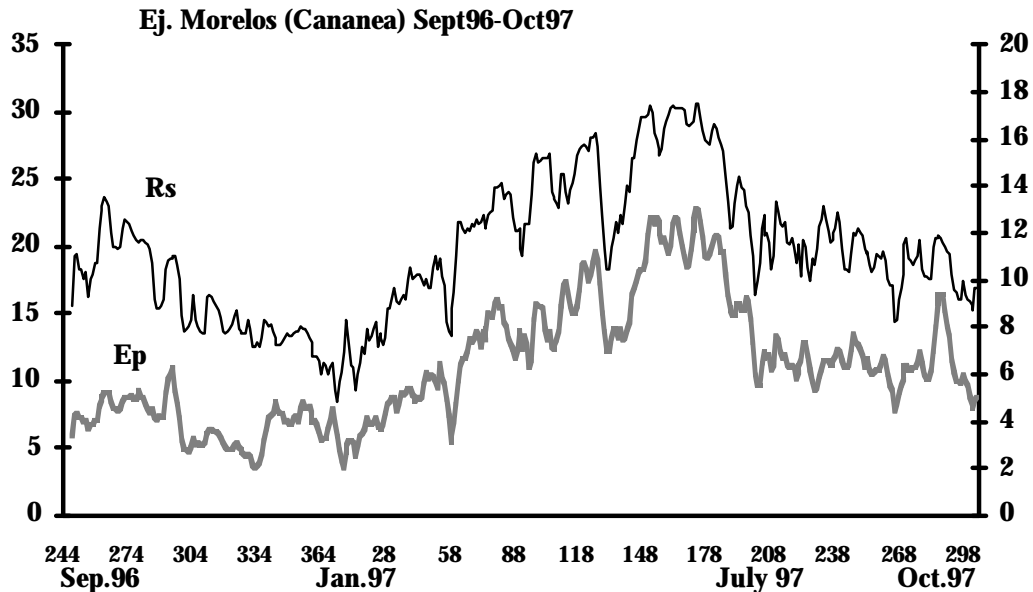


Fig : 4.2. Evolution of the incoming solar radiation Rs and the potential evaporation rate Ep at Morelos from September 1996 until October 1997.

The daily potential evaporation rate E_p is calculated by a formula developed by Lhomme (1998), based on the Penman equation. The increase of incident solar energy affects the evaporation rate from January to July. After, the reduction of E_p rates is larger than the decrease of the solar radiation in relation with the increase of the atmospheric water content. Fig 4.2 shows the evolution of the potential evaporation rate E_p and the solar radiation R_s , and Fig. 4.3 the evolution of the atmospheric water vapour pressure deficit ∂e together with the potential evaporation rate E_p .

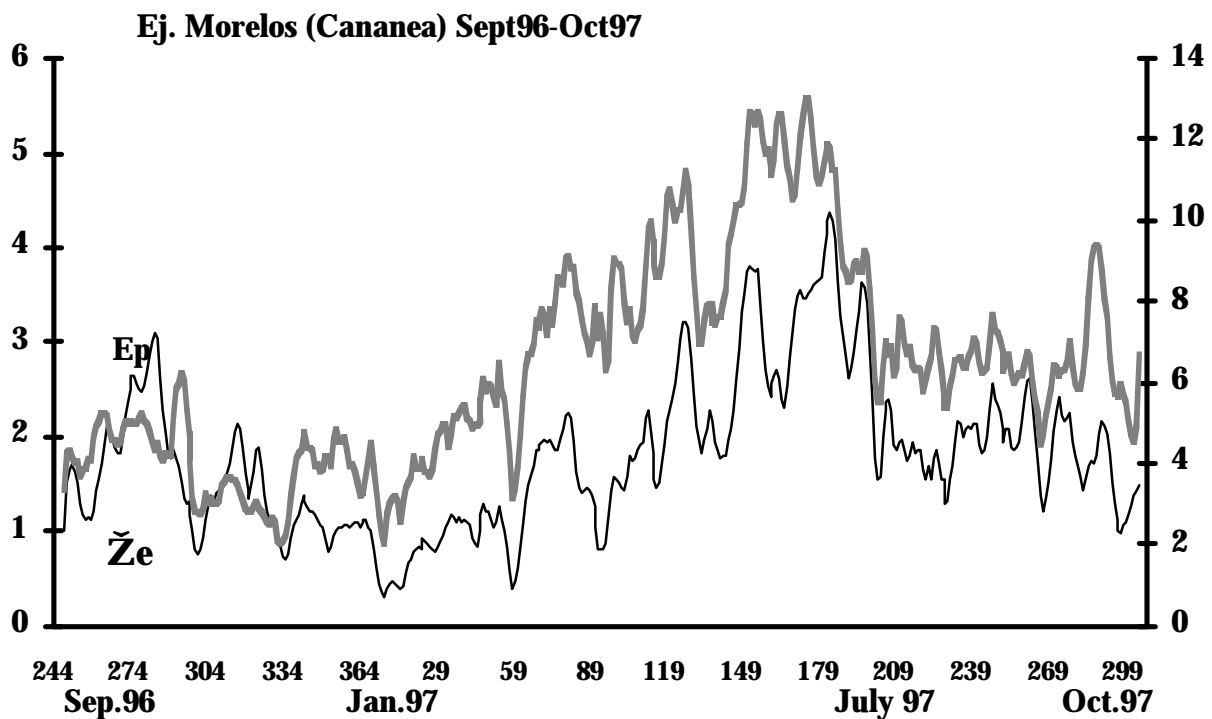


Fig. 4.3. Evolution of the potential evaporation and the atmospheric water vapour pressure from September 1996 to October 1997.

We observed that E_p decreases drastically during the month of July from 12mm/day to 6-7mm/day in relation with the reduction of the atmospheric water vapour pressure deficit ∂e , and partially with the decrease of solar radiation R_s . The reduction in climatic demand (R_s and ∂e) is related to the arrival of the "mexican monsoon" in the northern region of Sonora. In May (day 155-170), some preliminary rainfalls affected atmospheric water vapour content without decreasing the E_p rates. High-speed winds prevailed during this period.

In semiarid conditions, convective energy (water vapour pressure deficit) plays the same important role as available energy in the general climatic demand represented by the potential evaporation rate. This later rate is evaluated to 2440 mm/year, whereas convective energy represented 43 % of the total yearly amount.

4.2. Precipitation / soil moisture availability

Long-term mean July-September rainfall (1962-1985) was 204 mm at Naco and 289 mm at Cananea. During this summer, the rainy season was particularly short, with a total of only 224 mm of rainfall at our site in Morelos, mostly with amounts less than 4-8 mm and only eight large substantial events (>12 mm).

During the summer period, precipitation was mainly produced from convective cells initiated by surface heating, convergence and/or orographic lifting. Locally, thundershowers generally developed during the afternoon, due to a combination of high sensible heat fluxes at the soil-vegetation interface (see § 4.6.) and advected tropical moist air from the south, mainly from the Gulf of California. One major phenomenon associated with these convective clouds was lightning, which was very prevalent during their development. Most showers were of light/moderate intensity because droplets generally evaporated before reaching the ground surface. The result was highly spatiotemporally variable rainfall and thus soil moisture contents. Large thunderstorms affected mean air and surface temperatures.

Another interesting phenomenon involved the formation of a type of convective cell moving with the wind that produced a streaky precipitation distribution, parallel to the wind direction. The following example indicates the effect of this type of cloud on rainfall distributions: 12.5 mm of precipitation was recorded in the upper part of our transect, at the mesquite grassland site, while 37 mm was noted in the lower part, i.e. 5 km away in the grassland collector area. This level is threefold higher, and it occurred several times in the same year, and subsequently affected grassland biomass production throughout the region (§4.3.).

7 October 1997, a large outburst passed over the whole catchment area (Fig. 4.4.). Wind from the south brings Gulf moisture to the region. The rapid increase in wind speed to 11 ms^{-1} prior to rainfall is typical. The rainfall pattern is in the form of a monomodal dysimetric curve, with a high intensity rate at the beginning. The intensity was higher than the infiltration rate and produced runoff throughout the area. Flooding areas received so much runoff water that the Rio San Pedro swelled

quickly and flooded over riparian surfaces. The 3 GOES images represent daily variations in the water vapour concentration (in yellow/red) in the atmosphere at 1400 h. Outbursts formed when the wind blew humid air from the Pacific over the Sierra Madre Occidental.

Rainwater inputs in this semiarid region are characterized by the type of clouds :

= many small amounts of rainfall (3-8 mm) throughout the area from convection showers, irregularly and scattered both in space and time, or from convective cells moving with the wind;

= some large events such as storms from cumulo-nimbus clouds, sometimes with hail; on such occasions, they can induce large-scale runoff, affecting water distributions at the ground surface and producing considerable surface erosion;

= the period between events can be of considerable length and thus affect vegetation growth.

The dynamics of soil moisture potential over time, obtained through the automatic measurement system installed at the *Bouteloua* site, are presented in Fig. 4.5. It shows variations in the soil water potential at different depths just after a rainfall.

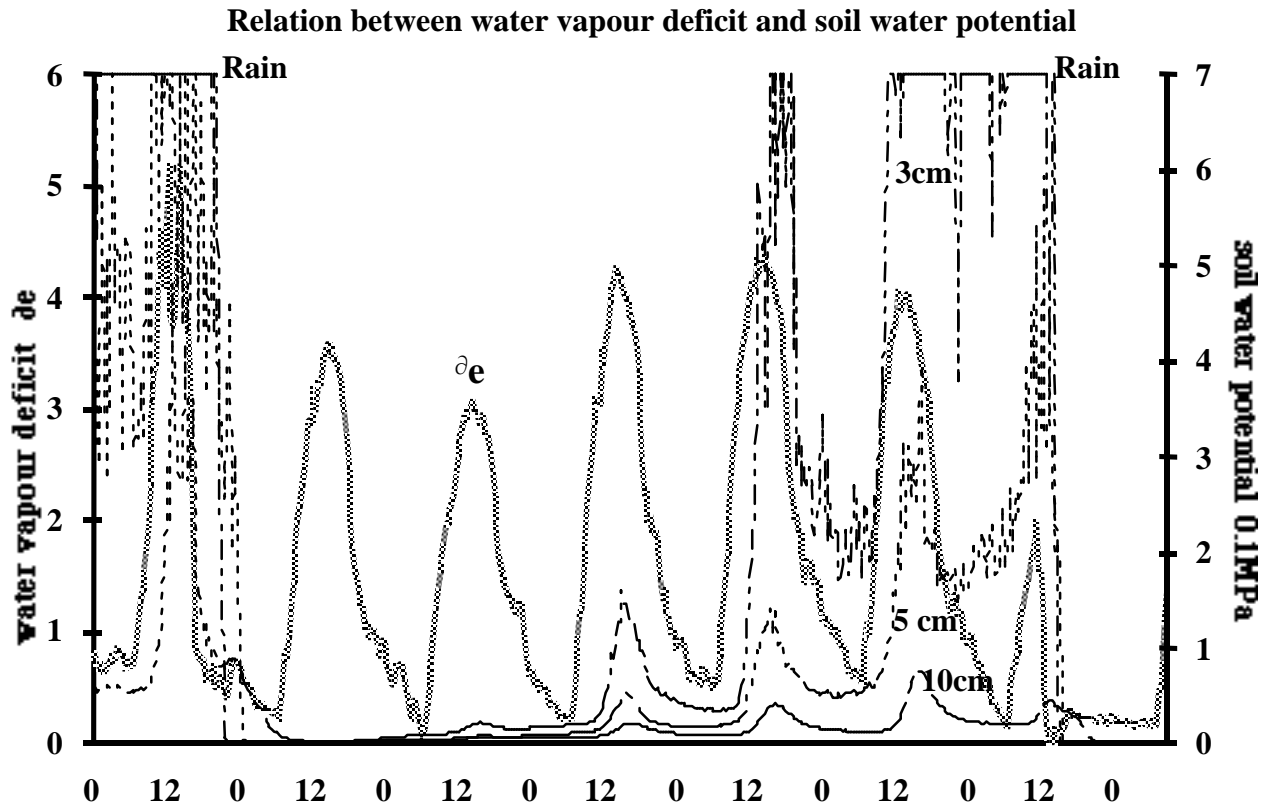


Fig. 4.5. : Daily course of soil water potential beginning just after a rain which saturates the soil upper layers and atmospheric demand ∂e .

The first day, rainfall was found to saturate the soil to approximately 20 cm depth. The soil water potential dropped to nearly zero, as measured the day after the event. The top 10 cm soil layer is characterized by a very rapid drying process: soil water potentials at 3-5 cm increase rapidly and more slowly at 10 cm. In less than 4 days, the first 5 cm soil layer was dry. The soil surface evaporation process was clearly observed and related to the atmospheric water vapour pressure deficit (∂e) (Fig. 4.5.). The sinusoidal course of the soil water potential resulted from high climatic demand (∂e) during the day and an unsaturated flow supply from the lower layers. At night, when climatic demand was low, the soil was partially replenished with moisture from the underlayers and the soil water potential declined.

The water potentials could be converted to water contents using the moisture tension release characteristics. Soil water potentials of -0.01MPa correspond to a soil water content of around 7-8% for the upper layer after percolation and 10-11% for 10-20 cm depth.

Soil water potentials near the surface (0-15 cm) varied consistently in response to individual rainfall events, which were generally of short duration, and to climatic demand. The soil evaporation process predominated in the dry grassland ecosystem and the mesquite grassland community due to the presence of large bare soil surfaces. In the wet grassland ecosystem, fluctuations in the soil water potential were less marked because of the vegetative soil cover and the quantity of organic matter present in the soil.

4.3. Vegetation : biomass production (kg/ha) tableau (with and without livestock)

Due to summer rainfall, 90-95% of the herbage biomass in the semidesert grassland (pastizals) is produced during the July to late September warm period.

The *Bouteloua* grassland was found to have 15-20% soil coverage, with a sparse grass layer of different species dominated by *Bouteloua gracilis*, *B. repens*, *Aristida ternipes* and sometimes patches of *Hillaria belangeri*. The grass layer is mainly composed of perennial plants, mostly C4 species with a few C3 species. The grasses generally have an erected-leaf structure. The grass cover is more complete in the wet *Bouteloua* grassland, with a higher clump density. Annual C3 plants are very common in this part, thus representing an important element in the general physiognomy of the landscape.

Grassland biomass production depends on the temporal and spatial rainfall distribution. When the rainy season started early and rainfall events were substantial enough to avoid long periods of water stress, the different species were able to grow "normally" to the seed production stage. In this semiarid region, the interstorm periods can be long enough to completely deplete the moisture in the top 20 cm of soil, where 80% of the root systems grow. The irregular rainfall distribution decreased the growth potential of the grass species as seedlings emerged. This year, the first rains of the summer season fell during two large storms occurring at 2-day intervals, which increased the spatial heterogeneity with respect to soil water availability in conjunction with the runoff process. Wet grasslands received more water in the lowlands. These communities have a higher growth potential, even with long drought spells, compared to other grassland communities growing on eroded gravelly upland sites. However, the wet grasslands did not receive sufficient runoff water this year (see photo September 1997). In the "mesa", these processes have led to a mosaic of different grassland habitats, which is a feature of this catchment area.

Table 4.2 gives some data on the areal dry matter production measured at different sites in the transect relative to total precipitation.

Table 4.2. : Areal grassland dry matter production (gr/m²) in relation with precipitation amount (with or without livestock) 1997.

	mesquite grassland	dry grassland bouteloua	wet grassland area
precipitation mm	116	176	215
Areal Biomass production (gm- 2)			
without livestock	65	78	135
with livestock	14	18	53
potential without livestock		114	204

The two dominant grasses of the semidesert grassland (*Bouteloua gracilis* and *B. repens*) form a perennial grass-scrub dominated landscape on gravelly upland sites and in wetter areas. They are associated with other perennial and annual grasses. Their growth dynamics, influenced by rainfall patterns, account for the physiognomy of the grass layer. Redistribution of rainwater through increased runoff has had an important role in the development of the physical environment. The dynamics of moisture contained in the top 20 cm of soil has to be taken into account when assessing grass growth processes, and thus in the evolution of the ecosystem. Total areal biomass production differed between years in relation to rainfall events and to the redistribution/infiltration of runoff water in the soil. For the same total amount of precipitation in summer, biomass production can be completely due to the differential dynamics of plant species induced by the distribution of rainfall events during the wet season.

4.4. Radiation budget over sparse grassland vegetation

The net radiation is affected by radiative surface properties as reflected and emitted radiation. Figure 4.6. presents temporal evolution of incoming solar radiation R_s , reflected radiation R_r , the emitted radiation and atmospheric radiation as well as radiation budget R_n .

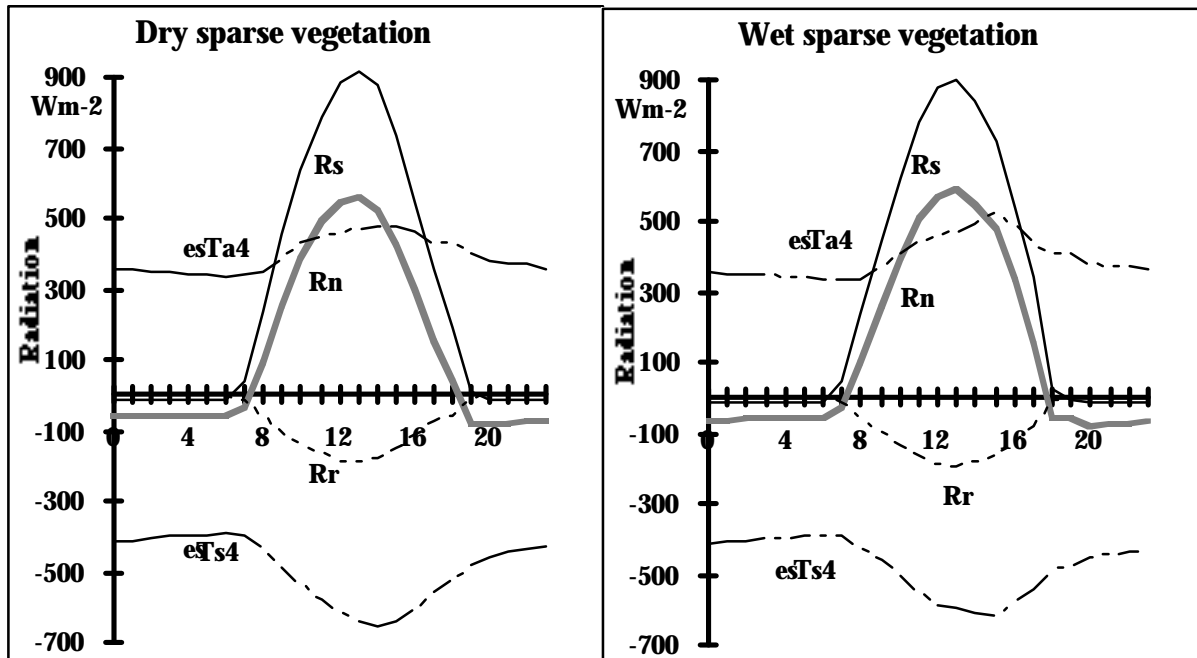


Fig. 4.6. Variations of the different components of the radiation budget over two grassland ecosystems.

In the summer period, the overall *Bouteloua* grassland albedo (R_r/R_s) was 22%, but varied according to the soil surface humidity.

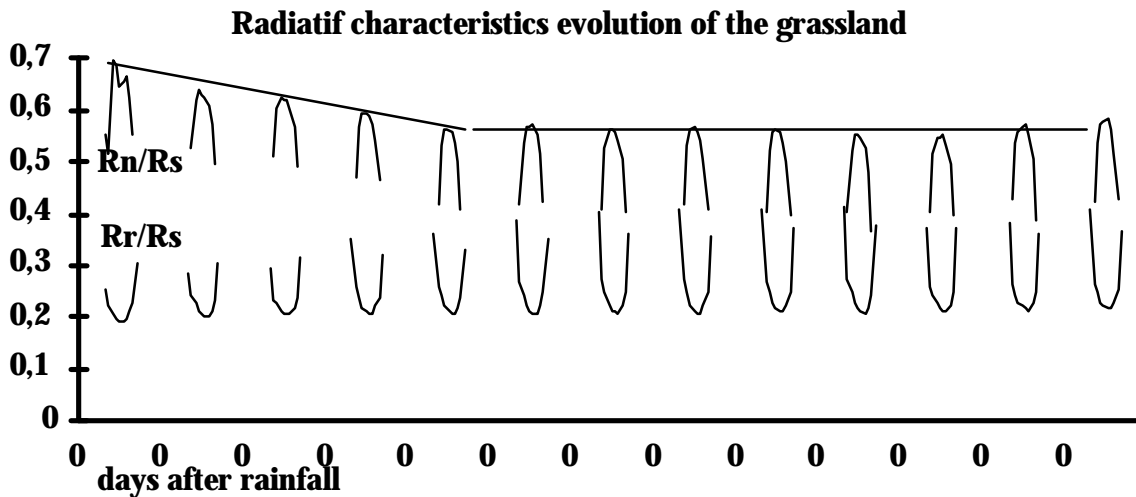


Fig. 4.7. Evolution in radiative surface properties : albedo (R_r/R_s) and net radiation over a grassland ecosystem.

The general albedo trend showed a progressive increase during the first 5 days, whereas the radiation budget pattern presented a more substantial decrease for both surfaces. The reduction was due to progressive drying out of the soil surface,

which in return induced an increase in soil surface temperatures. The radiation budget decreased proportionally to increases in long-wave radiation loss. Surface temperature, through emitted radiation $\epsilon\sigma T^4$, affects the radiation budget.

Surface properties affect the radiation budget. Surface soil moisture is the main factor affecting both reflected and emitted radiation. It is an important characteristic to be taken into account when analysing satellite images of the semiarid region taken in summer.

4.5. Available energy ($R_n - G$)

It is essential to accurately determine the available energy in order to be able to precisely evaluate turbulent exchanges between the soil-vegetation surface and the atmosphere. This is one of the most difficult tasks when conducting investigations over sparse vegetation, even if net radiation and soil heat flux density are measured directly with sensors. As presented in §3.2., for the purposes of this study, the mean soil heat flux was calculated by averaging data obtained from four soil flux plates dispersed over the grassland surface. For the radiation budget, one sensor was positioned at 9 m height in order to accurately estimate net radiation.

The daily courses of net radiation did not differ for the two grassland surfaces at the outset of the observation period. (fig.4.8.).

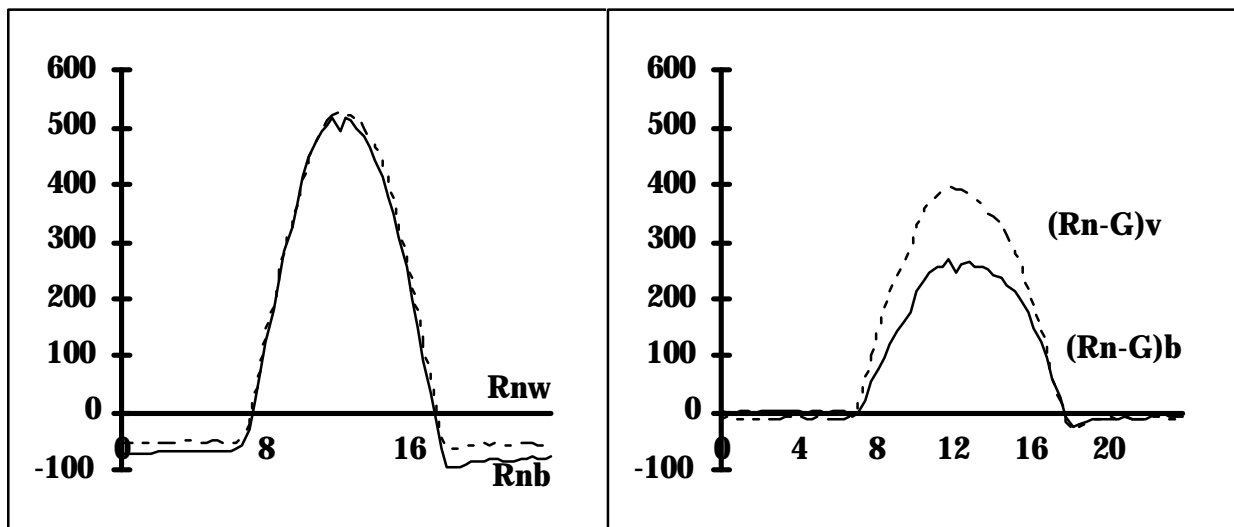


Figure 4.8. Daily variations in net radiation and available energy for the two grassland ecosystems.

The surface characteristics at this time were very similar (see photo). However, available energy ($R_n - G$) differed due to the high soil heat flux. The daily soil heat flux density was higher at the sparse dry *Bouteloua* grassland, consequently

reducing the available energy as compared to the other grassland site where some dry vegetation was still present.

In semi-arid conditions, it is essential to accurately measure the radiation budget and the convective soil heat flux due to the presence of large bare soil areas. The available energy of a sparse dry grassland can be 40% less than that of a more densely covered grassland. This reduction in available energy is very significant in the partitioning of sensible and latent heat fluxes.

4.6 Soil-vegetation-atmosphere interaction.

Surface fluxes of latent and sensible heat were measured using Bowen-ratio energy balance stations. However, prior to the intensive measurement period in this study (IOP), performances of the different instruments-sensors were tested for 3 weeks, and then the Bowen ratio stations were compared for 2 weeks at the Sonora Agricultural School near Hermosillo. The stations were located in close proximity in the same alfalfa field. The results of analyses of data collected with both devices to evaluate sensible and latent heat fluxes during the alfalfa growing period closely agreed.

The devices were then installed in June 1997 in the field near Ej. Morelos sites 2 and 3 (see map), and flux measurements began just after the first rains, at the onset of the grass growth cycle. Figure 4.9.a,b presents variations in energy flux densities measured in two different grasslands before and after a rain event.

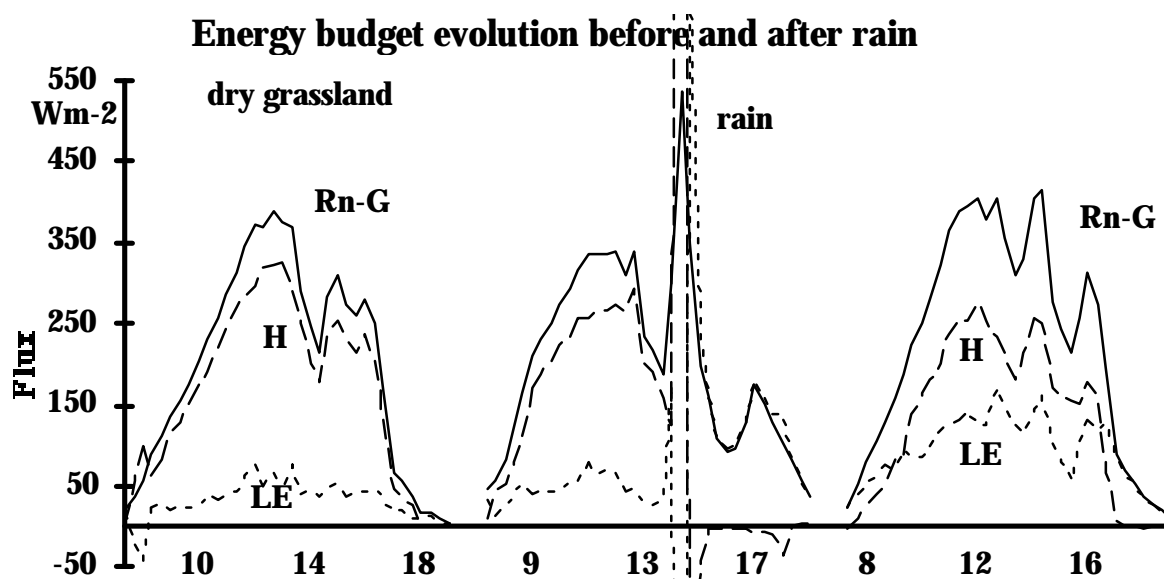


Fig. 4.9.a : Diurnal variations in available energy Rn-G, latent heat LE and sensible heat H in a dry *Bouteloua* grassland.

Daily levels of available energy measured over a 15-20% covered soil (Fig.4.9.a) were less than over a more densely vegetated surface, thus confirming earlier results. Just after a rain of 4 mm, latent heat was nearly equal to the available energy. Most of the latent heat flux was considered in terms of soil evaporation at the onset of the vegetation growth cycle at the sparsely vegetated grassland. Over time, the evaporation rate quickly dropped as the sensible heat increased.

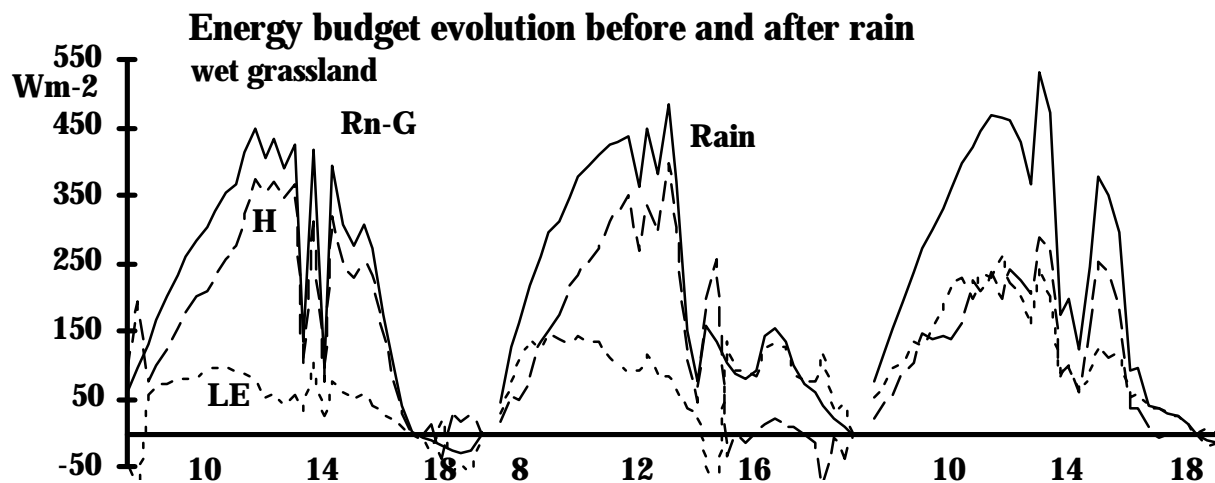


Fig. 4.9.b : Diurnal variation of the available energy Rn-G, latent heat LE and sensible heat H over a wet *Bouteloua* grassland.

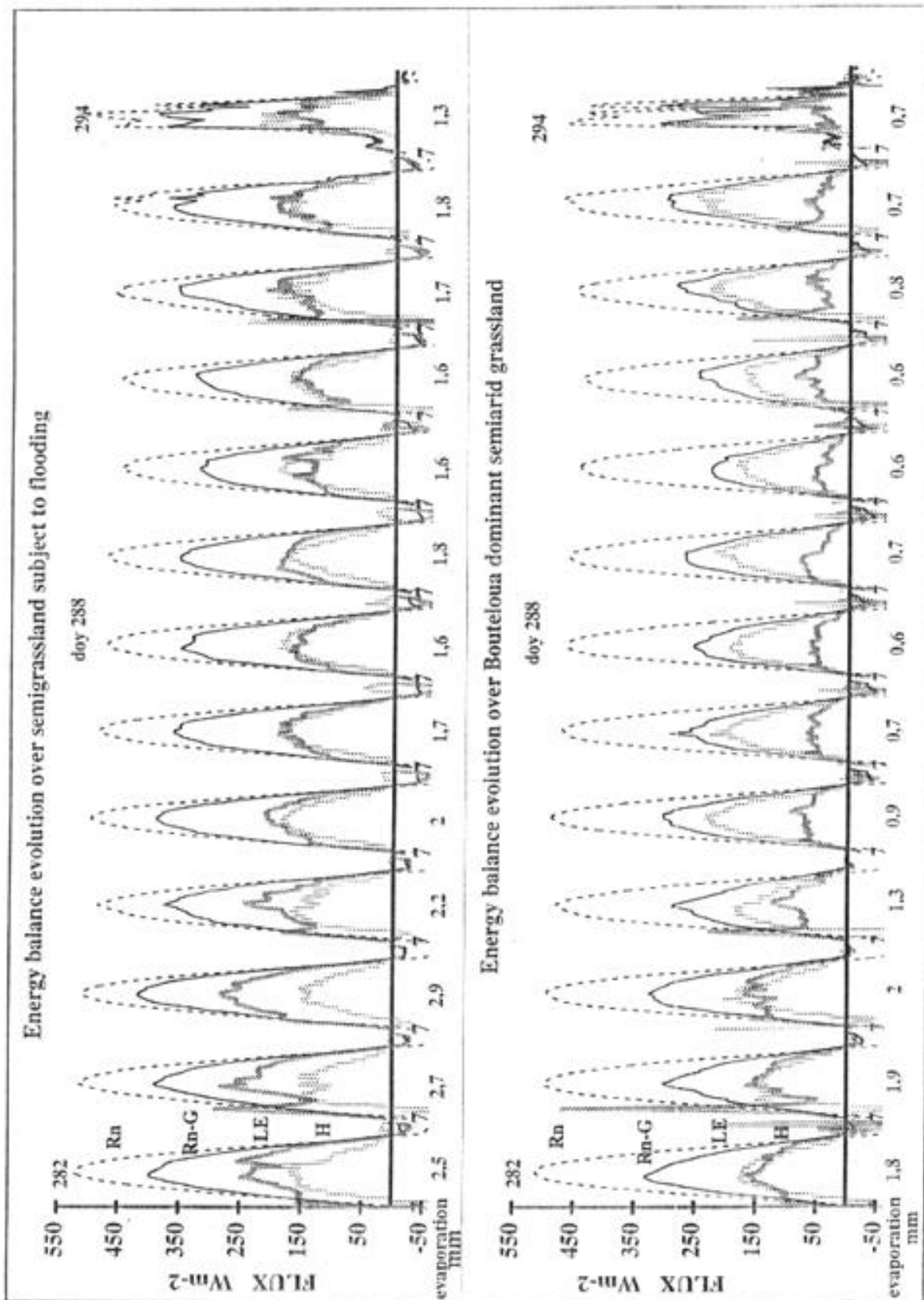
The evaporation reduction was less marked at the wet grassland site (Fig. 4.9.b) in relation to the vegetation cover. It was not possible to measure nocturnal latent heat flux densities due to the weakness of the water vapour gradient, which was the same magnitude as the sensor error.

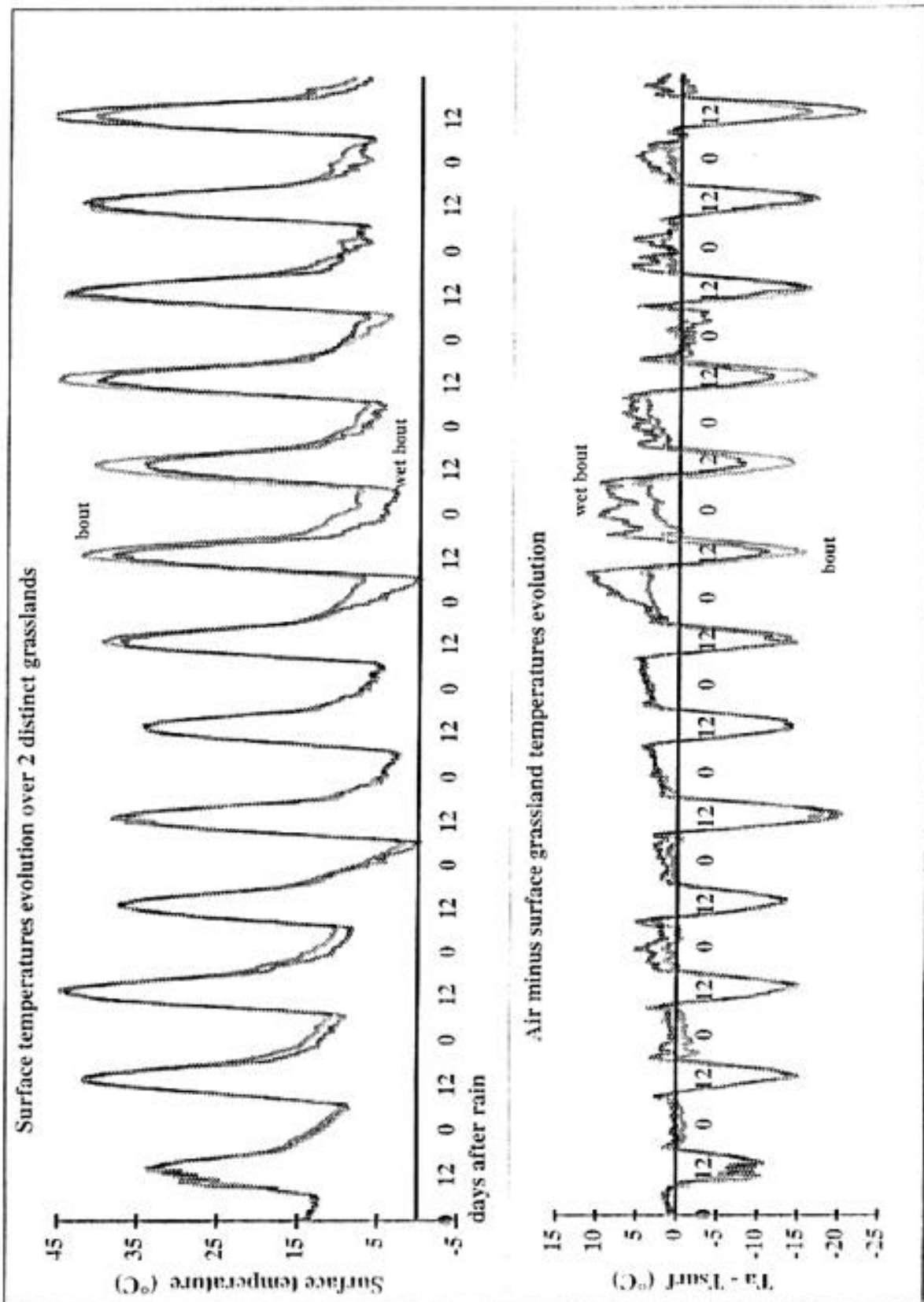
After 30 days, areal biomass production increased differently at the two sites (see § 4.3.). Variations in available energy and its partitioning into latent and sensible heat, as measured with the Bowen ratio method, over the two distinct vegetation surfaces for 13 days, are presented in Fig. 4.10. The measurements began just after a rain. There was a noticeable effect of the vegetative cover on available energy and on the sensible and latent heat components.

This highlighted:

- = higher available energy in the wet vegetated area as compared to the dry *Bouteloua* grassland site;

- = a steady decrease in the latent heat flux during the first days after a rain event, which was more marked over sparse *Bouteloua* grassland than over the wet vegetated grassland area. Sparsely vegetated surfaces dried out faster than the vegetated surface (see § 4.2.);
- = when dry, the bare soil surface offered much higher resistance to water transfer to the atmosphere, and most of the available energy was converted to conductive soil heat flux and to convective sensible heat flux. At the wet vegetated grassland, after the first days, available energy was almost equally partitioned between latent and sensible heat fluxes at this stage of grassland growth;
- = evaporation was twice as fast at the wet grassland in comparison to the dry *Bouteloua* grassland, which was related to the density and leaf area of the vegetation, available energy and the soil water content. The total amount of water returning to the atmosphere during this period was 25 mm in the wet grassland, compared to 13 mm at the dry grassland site during this period.





After 4-5 days of drying out, the surface temperature of the sparsely vegetated area progressively rose to a higher level than that of the vegetated surface. This increase was related to the reduction of soil evaporation, while vegetation evaporation remained relatively constant. The air to surface temperature difference highlighted that the surface temperature could range from 15 to 20° C and drop by 5-10° C at night (Fig. 4.11.). This is an important parameter for understanding how grasses can adapt to wide diurnal temperature fluctuations, particularly concerning the growth dynamics of young seedlings. It is also a very important factor for termites, which have an important role in the soil structure as well as in the redistribution of infiltrated water through tunnels in the soil.

Variations in the evaporative fraction $LE/R_n-G = EF$ in the two grassland ecosystems provide insight into the partitioning of available energy (Fig. 4.12), as represented by a ratio between the evaporation rate (LE) and available energy (Rn-G). It is generally acknowledged to be constant around midday. Daily variations can be attributed: 1. to advected energy which alters partition of available energy; and 2. to clouds which affect net radiation.

The EF levels started at 0.65-0.7 just after a rain and decreased for 5 days to 0.50 for the wet grassland and 0.30 for the dry grassland. This corresponds to the soil-surface related decrease in the evaporation process (*check*), and evaporation was more a vegetation process thereafter. The difference between the two grassland surfaces was attributed to the difference in areal biomass and to the soil water content.

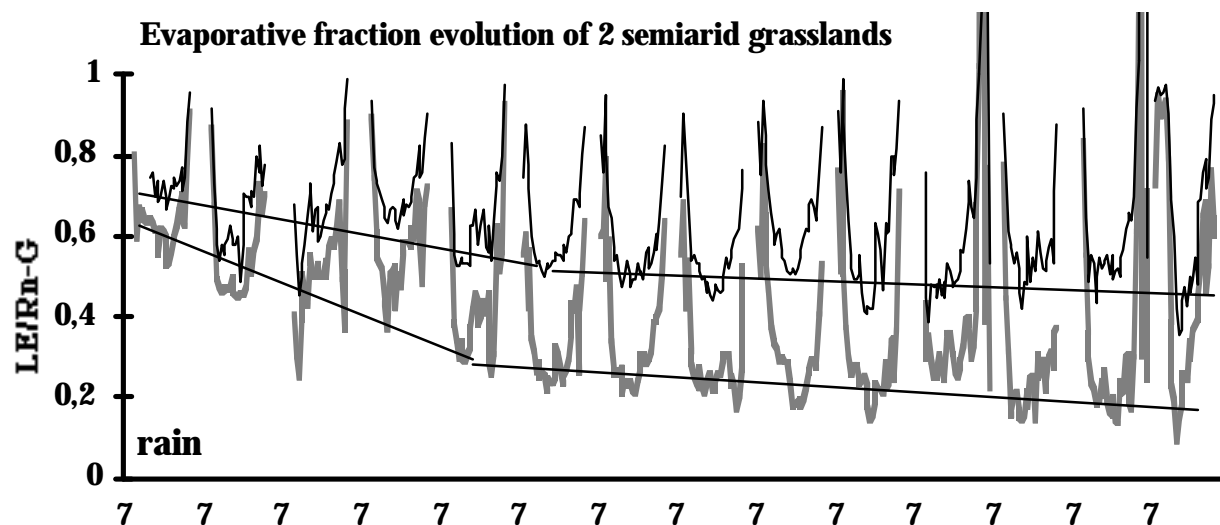


Fig. 4.12.: Variations in the evaporative fraction over two distinct grassland surfaces for 13 days after a rainfall.

Observed differences in sensible and latent heat fluxes over the semiarid grasslands were due to:

1. higher available energy levels at the wet vegetated grassland site than at the dry grassland site;
2. the soil moisture content and stage of growth in the wet grassland promoted higher evaporation rates for a longer period of time;
3. low evaporation rates were related to the low level of water infiltration into the soil and to the patchiness of the grass cover;
4. high surface temperatures were recorded a few days later after rainfall; the wetness and drying out cycle induced the formation of a crust at the soil surface, thus affecting the seedling and soil fauna dynamics.

Sensible heat flux was evaluated by an independent method involving measurement of the standard deviation for temperature, or the σT method (§3.6.2.). The aim of this strategy was to verify data obtained by the Bowen ratio method. However, it was shown that the temperature fluctuation method is only valid if used under certain specific conditions. Over heterogeneous surfaces of a patchy vegetation, there can be considerable spatial variability in turbulence over a wide range of scales. When the upwind is blowing regularly from one direction over a relatively large "homogeneous" surface, the surface layer can be stabilized.

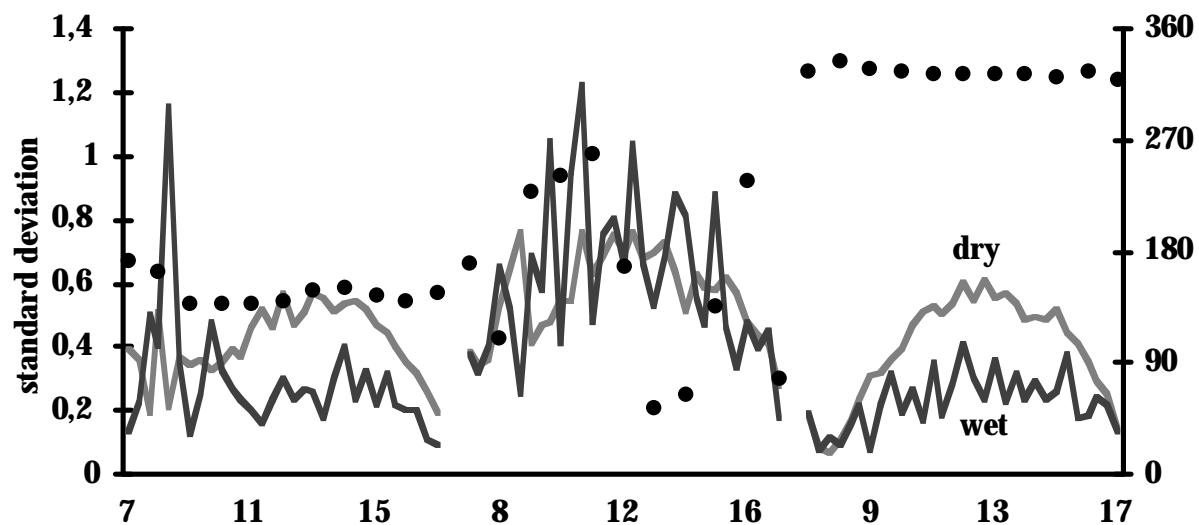


Fig. 4.11. Daily variations in the standard deviation measured at 1.4 m height above the surface of two grasslands in relation to the wind direction.

The effective sources and sinks of the upstream surface more or less "constantly" contribute to the turbulent exchange processes. The source area is an important factor which renders the standard deviation of the air temperature (σT) significant. Fig 4.11. shows variations in σT for 3 days over the two grassland systems. When the wind was from approximately the same direction, as on day 1 (from the south) or day 3 (from the north), diurnal variations in σT were in line with diurnal net radiation variations.

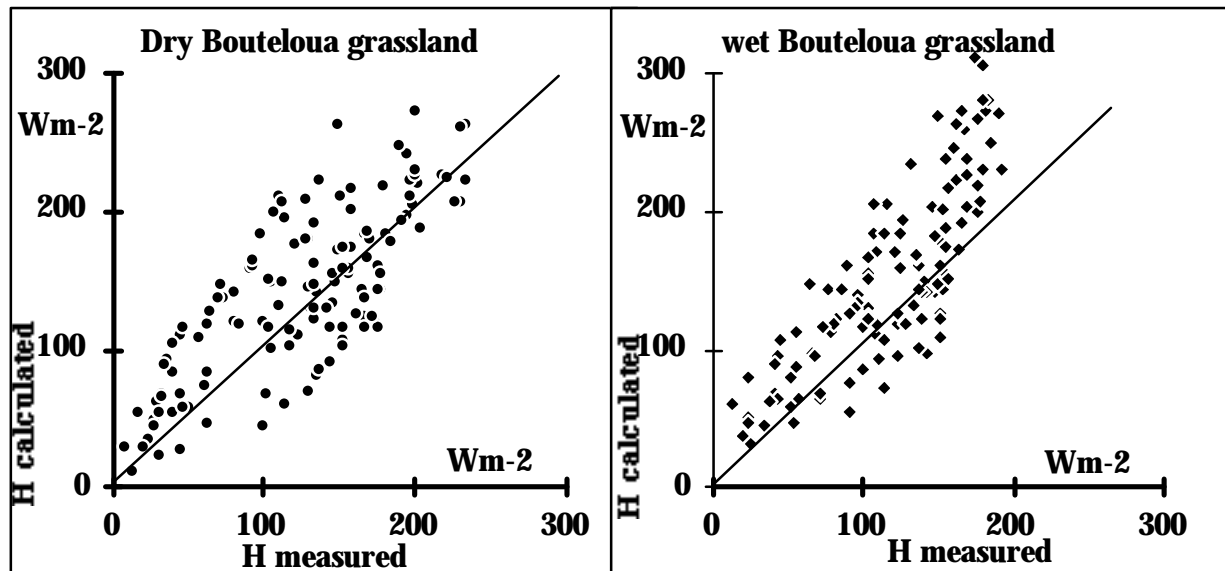


Fig. 4.12. Comparison between the sensible heat flux obtained by the Bowen ratio method (M measured) and the sensible heat evaluated by the σT method.

The drier the surface, the higher the standard deviation for temperature, i.e. the broadest temperature variation was noted on a dry surface. The σT variations above the wet surface could be attributed to the patchiness of the vegetation cover (see photo taken 3 weeks prior to collection of the present data).

An unstable wind direction affected the σT values for temperature, as observed on the second day. This was more perceptible over the wet surface, possibly due to marked unstable air stratification over patchy areas. Comparison with data obtained by the Bowen ratio method is difficult under variable wind direction conditions. Fig. 4.12 shows the relation between the sensible heat flux obtained with the Bowen ratio system and the calculated sensible heat values measured by the sigma T method.

REFERENCES

- Goodrich, D. C. 1994 - SALSA-Mex : A large scale Semi-Arid Land Surface Atmosphere Mountain experiment. Proc. Intern. Geoscience and Remote Sensing Symp. (IGARSS '94) 1 :190-193. Aug. 8-12, 1994.
- Lhomme, J.P. 1997 - Towards a rational definition of potential evaporation. Hydrology and Earth System Sciences 2: (in press)